Algebraic and numerical studies on the roles of momentum conservation and self-adjointness in moment-based neoclassical particle fluxes

Cite as: Phys. Plasmas **30**, 092305 (2023); doi: 10.1063/5.0164313
Submitted: 22 June 2023 · Accepted: 24 August 2023 ·
Published Online: 18 September 2023

M. Honda[a)]

AFFILIATIONS

Graduate School of Engineering, Kyoto University, Kyoto 615-8530, Japan

[a)]Author to whom correspondence should be addressed: honda.mitsuru.5c@kyoto-u.ac.jp

ABSTRACT

Linearized collision operators are model operators that approximate the nonlinear Landau collision operator, but cannot capture all the features of the Landau operator. Various linearized collision operators have been proposed, including the one that ensures the self-adjointness of the operator and another that maintains the friction–flow relations derived from the exact linearized collision operator. To elucidate the basis for choosing an appropriate model operator that derives the matrix elements used to express the friction forces, the roles of momentum conservation and the self-adjointness of the collision operator in the neoclassical particle flux are investigated theoretically, algebraically, and numerically within the framework of the moment method. Linear algebraic calculations confirm that ambipolarity only requires the property of momentum conservation, while the self-adjointness is additionally necessary to ensure the independence of poloidal flow and particle flux from the radial electric field, which must be established in an axisymmetric system. This fact is also numerically validated by the one-dimensional fluid-based transport code TASK/TX, extended to handle impurity species, and the moment-method-based neoclassical transport code Matrix Inversion. In tokamak experiments, where a parallel electric field is typically present, it induces the inward Ware flux, where even electrons can have the same or larger particle flux as main ions and impurities. The Ware flux can significantly contribute to the total neoclassical particle flux, highlighting the importance of considering the electron flux when modeling neoclassical impurity fluxes.

I. INTRODUCTION

Controlling the particle balance in the core plasma region of tokamaks is critically important for achieving a steady state. In a steady state, the particle supply to and particle transport from the core region must be balanced for each species. Currently, particle supply systems such as pellet injection, gas jet, gas puffing, and neutral beam injection (NBI) effectively play a role by supplying the same amount of particles that are transported outboard of the plasma. However, in ITER and DEMO plasmas, which have larger volumes and higher densities and temperatures compared to current experiments, direct fueling to the core becomes challenging. Hydrogen isotopes need to be transported from the edge to the core regions to sustain a burning plasma state, as they are constantly lost in the core due to fusion reactions. In other words, the condition should be maintained where deuterium and tritium are transported inward, while helium ashes move outward.[1] From the perspective of achieving high performance, not only for burning plasmas but also plasmas in general, it is favorable to have a density profile that peaks toward the magnetic axis, keeping the Greenwald density fraction below one in the edge region while attaining it above one in the core. These facts emphasize the need to understand particle transport physics precisely. Particle transport has been less well understood than heat transport, partly due to the difficulty in estimating particle sources involving neutrals. However, in recent years, significant progress has been made in theoretical understanding, experimental comparisons, and model development.[2]

Turbulent and neoclassical transport play a crucial role in determining particle fluxes. The focus in this study is on neoclassical transport. The theoretical foundation of neoclassical transport was established half a century ago.[3,4] The moment approach, which utilizes ordered moment equations obtained by integrating the drift-kinetic equations multiplied by velocities,[5] has enabled neoclassical calculations with fairly high accuracy and speed. Its numerical implementations[6,7] have become prevalent for quantitative experimental analyses and have been incorporated into integrated transport models. In recent years, with advancements in computer performance, codes that directly solve local drift kinetic equations[8,9] or global drift kinetic equations[10–14] have been developed and utilized for these purpose. Additionally, neoclassical transport theory has been extended to include the effects of large flows,[15] heavy impurities,[16,17] plasma rotation,[17] poloidal asymmetry,[16,18] and neoclassical toroidal viscosity arising from toroidal asymmetry or three-dimensional geometry.[19,20] Furthermore, efforts have been made to improve the linearized model collision operator.[21,22]

As such, neoclassical theory has been extended by relaxing some of the physical assumptions previously made. However, the moment method has proven capable of reproducing many fundamental phenomena derived from the neoclassical transport theory quite well. Consequently, numerical implementations of the moment method, such as Matrix Inversion (MI)[6,23,24] and NCLASS,[7] remain widely used, particularly in integrated transport models (e.g., see Refs. 25–29). In the moment method, the collision operator is velocity-integrated to obtain the matrix elements, which are the essential components of the friction coefficients and viscosity coefficients. The combination of the friction coefficients and the generalized flows describes the friction forces, and this relationship is known as the friction–flow relations.[5] The choice of model collision operator in the drift kinetic equation influences the moment method through these matrix elements. The initial model collision operator used in the original moment method paper[5] was designed to conserve momentum but not the self-adjointness.[30] This model collision operator is only approximately self-adjoint for the different masses and temperatures, although it still guarantees momentum conservation.[24,31,32] The self-adjointness ensures symmetry in the matrix elements and friction coefficients, while momentum conservation results in ambipolarity of neoclassical particle fluxes. Violating the self-adjointness could introduce nonphysical problems, so the actual numerical implementation devised a method to enforce symmetry in the friction coefficients by ensuring symmetry in the matrix elements.[7,24] Recently, as the need to handle multi-species plasmas has grown, drift kinetic solvers have been updated to incorporate the exact linearized collision operator.[33–35] The velocity-space moments of the exact linearized collision operator have been proposed as applicable to any arbitrary mass and temperature ratios,[31,32] and they have been numerically implemented in MI.[24] The matrix elements derived from the exact linearized operator maintain momentum conservation but do not generally preserve the self-adjointness;[31,32] however, the self-adjointness holds when the temperatures of colliding particles are equal.

The exact linearized collision operator itself does not satisfy the self-adjointness.[21] Therefore, a linearized model collision operator for multi-species plasmas has been proposed, which conserves particles, momentum, and energy while satisfying the self-adjointness. This operator, commonly referred to as the Sugama operator (named after the developer), remains valid even for collisions between unlike species with unequal temperatures.[21] However, the field-particle part of the Sugama operator diverges from that of the exact operator in a high collisionality regime. To address this drawback, two types of improved model collision operators have been developed.[22] The first one is the improved Sugama operator, which can reproduce the same friction–flow relations as those given by the exact linearized collision operator. However, the self-adjointness is only *approximately* valid for collisions between unlike species with unequal temperatures. The other is the *modified* improved Sugama operator, which exactly satisfies the self-adjointness but yields friction coefficients that deviate slightly from those given by the exact operator. The matrix elements of the friction coefficients for both models are provided in Ref. 22 and are readily available for implementation in a code based on the moment method. The paper does not provide a clear guideline regarding which model to use, so the choice must be made based on the specific purpose or, in other words, whether to prioritize the self-adjoint property.

In tokamak plasmas, ambipolarity is a crucial property. Both turbulent and neoclassical particle fluxes must be individually ambipolar; otherwise, the radial current torque, known as the $\boldsymbol{j} \times \boldsymbol{B}$ torque, would induce toroidal rotation in the plasma. Here, $\boldsymbol{j}$ and $\boldsymbol{B}$ represent the current density and the magnetic field, respectively. Due to the transport ordering, conventional transport codes explicitly assume quasi-neutrality, and the density of at least one species, typically electrons, is determined based on the quasi-neutrality condition. That is, in this case, the particle transport equation for electrons is not solved, and the electron particle flux needs to be determined based on the ambipolar condition. In other words, the ambipolar condition is automatically satisfied and typically does not pose a concern. In contrast to conventional transport codes, the one-dimensional fluid-based transport code TASK/TX solves a set of equations analogous to the two-fluid model for all particle species.[36,37] The governing equations, derived using the drift ordering, are flux-surface averaged. The unique aspect of this code is that it does not impose quasi-neutrality and ambipolarity forcibly. Instead, quasi-neutrality and ambipolarity are naturally achieved as a result of the physical models implemented in the code, such as the friction coefficients, rather than through enforced conditions. Consequently, the use of friction coefficients that do not satisfy ambipolarity can lead to non-ambipolar neoclassical fluxes, which in turn result in spurious toroidal rotation due to the $\boldsymbol{j} \times \boldsymbol{B}$ force. Another essential property in an axisymmetric system like a tokamak is that the particle fluxes and the poloidal flows should not depend on the radial electric field E_r:[5,38] E_r should not influence transport. In conventional transport codes where quasi-neutrality is forcibly imposed, E_r is typically determined by the radial force balance equation. However, strictly speaking, this is inconsistent since the static E_r originates from a slight imbalance in charge densities. In TASK/TX, E_r satisfies both the radial force balance and the slight charge density imbalance. These facts clearly demonstrate that the TASK/TX system is highly autonomous, and any slight inconsistency can potentially lead to a breakdown of physical soundness. Thus, selecting an appropriate physics model is indispensable for a system like TASK/TX to maintain its physical integrity. Therefore, it is necessary to scrutinize the relationship between these features and the self-adjointness.

TASK/TX was originally developed assuming a pure plasma. While it was capable of handling neutrals and fast ions generated by NBI, it only considered electrons and main ions when it came to charged thermal particles. However, recent extensions to TASK/TX now include impurity species among the thermal species. The focus is primarily on fully stripped carbon species, as they are the main impurity species in the current experimental device, such as JT-60U. This extension allows for the examination of ambipolarity in the neoclassical particle fluxes, not only in MI but also in TASK/TX, since the behavior of neoclassical particle fluxes significantly differs between a pure plasma and an impure plasma. In a pure plasma, the electron particle flux must be balanced with the ion particle flux to satisfy the ambipolar condition, i.e., $\Gamma_e^\psi = \Gamma_i^\psi$. However, in an impure plasma, it is usually assumed that the electron particle flux becomes negligible due to the disparate mass ratio, and the main ion and impurity fluxes are balanced ($\Gamma_e^\psi \ll \Gamma_i^\psi \approx Z_I \Gamma_I^\psi$).[5,16] Here, $\Gamma_a^\psi \equiv \langle \boldsymbol{\Gamma}_a \cdot \nabla\psi \rangle$ represents the contravariant component of the particle flux for species a, $\boldsymbol{\Gamma}_a$, where $\langle \cdots \rangle$ denote the flux surface average, ψ is the poloidal flux function, Z is the charge number, and e, i, and I refer to the electron, main ion, and impurity species, respectively. The neoclassical impurity flux is typically modeled based on the relation $\Gamma_I^\psi \approx Z_I^{-1} \Gamma_i^\psi$ using the main ion thermodynamic forces.[16,18] However, these discussions did not account for the presence of the parallel electric field $E_\parallel$, which is almost always present in tokamak experiments as long as the Ohmic current flows, or in other words, when a one-turn or loop voltage $V_{\rm loop}$ is applied. As will be discussed in detail later, the Ware fluxes, which are a part of the banana-plateau fluxes, must emerge for any species including electrons, whenever $E_\parallel$ exists. The electron Ware fluxes could be comparable to or even greater than the fluxes driven by the thermodynamic forces, depending on the specific situations. If the Ware particle flux is significant in tokamak plasmas, it is not always reasonable to model Γ_I^ψ from Γ_i^ψ by assuming that Γ_e^ψ is negligibly small. The parallel, toroidal, and radial flows, as parts of the dependent variables of the governing equations, are self-consistently solved in TASK/TX, allowing for the natural occurrence of neoclassical transport. Consequently, there is no need to implement neoclassical transport models such as MI and NCLASS within TASK/TX. In other words, the neoclassical particle fluxes in TASK/TX can be compared with those calculated by the neoclassical transport models. To ensure the soundness of the calculations, the neoclassical particle fluxes calculated in TASK/TX using the same friction and viscosity coefficients as those used in MI will be compared directly with the fluxes calculated by MI. This comparison also aims to investigate the conditions required for ambipolarity and to assess the impact of the Ware flux.

The remaining sections of the paper are organized as follows: In Sec. II, we revisit the theoretical expression of fluxes within the framework of the moment method. Next, in an axisymmetric system, we rigorously demonstrate the necessary conditions for ambipolarity and the independence of poloidal flows and particle fluxes from E_r using linear algebra. It is crucial to provide a mathematical proof of these conditions rather than relying solely on numerical analysis, as it guarantees their validity in all situations. Section III explains the extension of TASK/TX to handle impurity species. In Sec. IV, we compare the neoclassical particle flux between TASK/TX and MI, focusing on the relative impact of the electron particle flux compared to the main ion and impurity fluxes, with particular emphasis on the Ware flux. Finally, Sec. V presents the conclusions and outlines future perspectives.

II. THEORETICAL FOUNDATION OF CROSS-FIELD PARTICLE FLUXES AND AMBIPOLARITY

A. Friction–flow relations

First, we will revisit the fundamental formulation of neoclassical transport, which is necessary in Secs. II B–II E. The notations used in the following are primarily based on those introduced in Hirshman's review paper.[5] By projecting the momentum and heat flux equations in the toroidal direction and neglecting the subdominant terms, we can derive the following flux-friction relations in axisymmetric systems:

$$\langle \boldsymbol{\Gamma}_a \cdot \nabla\psi \rangle = -\frac{1}{e_a}\langle R^2 \nabla\zeta \cdot (\boldsymbol{F}_{a1} + e_a n_a \boldsymbol{E}) \rangle, \tag{1}$$

$$\frac{1}{T_a}\langle \boldsymbol{q}_a \cdot \nabla\psi \rangle = -\frac{1}{e_a}\langle R^2 \nabla\zeta \cdot \boldsymbol{F}_{a2} \rangle, \tag{2}$$

where $\boldsymbol{q}_a$, $\boldsymbol{F}_{a1}$, $\boldsymbol{F}_{a2}$, e_a, n_a, and T_a represent the heat flux, particle friction force, heat friction force, charge, density, and temperature for particle species a, respectively. In general, the particle and heat fluxes, $\boldsymbol{\Gamma}_a$ and $\boldsymbol{q}_a$, are obtained by integrating the particle distribution function f_a in the velocity space as

$$\boldsymbol{\Gamma}_a = \int \boldsymbol{v} f_a \, d\boldsymbol{v}, \tag{3}$$

$$\frac{\boldsymbol{q}_a}{T_a} = \int \boldsymbol{v}\left(\frac{m_a v^2}{2T_a} - \frac{5}{2}\right) f_a \, d\boldsymbol{v}, \tag{4}$$

where v, $\boldsymbol{v}$ are microscopic particle speed and velocity, and m_a represents the particle mass. $\boldsymbol{F}_{a1}$ and $\boldsymbol{F}_{a2}$ are defined using the collision operator C_a as

$$\boldsymbol{F}_{a1} = m_a \int \boldsymbol{v} C_a(f_a) \, d\boldsymbol{v}, \tag{5}$$

$$\boldsymbol{F}_{a2} = m_a \int \boldsymbol{v}\left(\frac{m_a v^2}{2T_a} - \frac{5}{2}\right) C_a(f_a) \, d\boldsymbol{v}. \tag{6}$$

The neoclassical fluxes stem from the gyrotropic part of f_a. $\boldsymbol{E}$ denotes the electric field, while ζ and R are the toroidal angle coordinate and major radius, respectively. Applying the identity, which holds in the axisymmetric configuration,

$$R^2 \nabla\zeta = \frac{I}{B^2}\boldsymbol{B} - \frac{\boldsymbol{B} \times \nabla\psi}{B^2}. \tag{7}$$

Equation (1) turns out to be

$$\begin{aligned}
\langle \boldsymbol{\Gamma}_a \cdot \nabla\psi \rangle = &-\frac{I}{e_a}\Bigg\langle \frac{BF_{a1\parallel} + e_a n_a B E_\parallel}{\langle B^2 \rangle} \\
&+ \frac{1}{B^2}\left(1 - \frac{B^2}{\langle B^2 \rangle}\right)(BF_{a1\parallel} + e_a n_a B E_\parallel) \Bigg\rangle \\
&+ \frac{1}{e_a}\left\langle \frac{\boldsymbol{B} \times \nabla\psi}{B^2} \cdot \boldsymbol{F}_{a1} + e_a n_a \frac{\boldsymbol{B} \times \nabla\psi}{B^2} \cdot \boldsymbol{E} \right\rangle, \\
= &-\frac{I}{e_a \langle B^2 \rangle}\langle BF_{a1\parallel} + e_a n_a B E_\parallel \rangle - \frac{I}{e_a}\left\langle \frac{F_{a1\parallel}}{B}\left(1 - \frac{B^2}{\langle B^2 \rangle}\right) \right\rangle \\
&+ \frac{1}{e_a}\left\langle \frac{\boldsymbol{B} \times \nabla\psi}{B^2} \cdot \boldsymbol{F}_{a1} \right\rangle - I n_a \left\langle \frac{E_\parallel}{B}\left(1 - \frac{B^2}{\langle B^2 \rangle}\right) \right\rangle \\
&+ \left\langle n_a \frac{\boldsymbol{E} \times \boldsymbol{B}}{B^2} \cdot \nabla\psi \right\rangle, \\
\equiv &\langle \boldsymbol{\Gamma}_a^{\rm BP} \cdot \nabla\psi \rangle + \langle \boldsymbol{\Gamma}_a^{\rm PS} \cdot \nabla\psi \rangle + \langle \boldsymbol{\Gamma}_a^{\rm CL} \cdot \nabla\psi \rangle \\
&- I n_a \left\langle \frac{E_\parallel}{B}\left(1 - \frac{B^2}{\langle B^2 \rangle}\right) \right\rangle + \left\langle n_a \frac{\boldsymbol{E} \times \boldsymbol{B}}{B^2} \cdot \nabla\psi \right\rangle.
\end{aligned} \tag{8}$$

Here, I denotes the poloidal current function. The superscript "BP" represents the banana-plateau component of the neoclassical fluxes dominant in the long mean free path regime, "PS" represents the Pfirsch–Schlüter component effective in the collisional regime, and

"CL" refers to the classical flux. The banana-plateau flux is primarily driven by surface-averaged pressure anisotropies, as explained in detail later. As is clear from the definitions in Eq. (8), the Pfirsch–Schlüter flux arises from the poloidal variation of the friction forces on a magnetic flux surface, while the classical flux is driven by friction forces perpendicular to the magnetic field. If the collision operator satisfies momentum conservation, $\sum_a \boldsymbol{F}_{a1} = 0$ holds, and it is evident from Eq. (8) that each particle flux becomes ambipolar. In the following, we will confirm in detail that ambipolarity actually holds due to momentum conservation by expressing the friction forces in terms of flows. The fourth and fifth terms in Eq. (8) describe the motion of magnetic flux surfaces and the small classical $\boldsymbol{E}\times\boldsymbol{B}$ radial pinch,[5] respectively. It is worth noting that assuming quasi-neutrality would cause these terms to vanish when evaluating ambipolarity; hence, they are neglected in the subsequent derivation.

Equation (2) can also be reduced in a similar manner,

$$\begin{aligned}\frac{1}{T_a}\langle \boldsymbol{q}_a\cdot\nabla\psi\rangle &= -\frac{I}{e_a\langle B^2\rangle}\langle BF_{a2\|}\rangle - \frac{I}{e_a}\left\langle \frac{F_{a2\|}}{B}\left(1-\frac{B^2}{\langle B^2\rangle}\right)\right\rangle \\ &\quad + \frac{1}{e_a}\left\langle \frac{\boldsymbol{B}\times\nabla\psi}{B^2}\cdot\boldsymbol{F}_{a2}\right\rangle, \\ &\equiv \frac{1}{T_a}\langle \boldsymbol{q}_a^{\mathrm{BP}}\cdot\nabla\psi\rangle + \frac{1}{T_a}\langle \boldsymbol{q}_a^{\mathrm{PS}}\cdot\nabla\psi\rangle + \frac{1}{T_a}\langle \boldsymbol{q}_a^{\mathrm{CL}}\cdot\nabla\psi\rangle.\end{aligned} \tag{9}$$

The friction forces can be expressed in terms of the friction coefficients and flows, which is known as the friction–flow relation. The particle and heat friction forces are given as

$$\boldsymbol{F}_{a1} = \sum_b\left(\ell_{11}^{ab}\boldsymbol{u}_b - \frac{2}{5}\ell_{12}^{ab}\frac{\boldsymbol{q}_b}{p_b}\right), \tag{10}$$

$$\boldsymbol{F}_{a2} = \sum_b\left(-\ell_{21}^{ab}\boldsymbol{u}_b + \frac{2}{5}\ell_{22}^{ab}\frac{\boldsymbol{q}_b}{p_b}\right), \tag{11}$$

where $\boldsymbol{u}$ and $\boldsymbol{q}$ represent the particle and heat flows, respectively. The symbol ℓ_{ij}^{ab} denotes the friction coefficient between species a and b,[5] and p refers to the pressure. It is possible to include higher-order flow components in these relations without modifying the expressions of the equations.[5,24] For simplicity, we will not explicitly consider them in the following derivation, unless otherwise specified. If the collision operator used to derive the friction coefficients ensures momentum conservation,

$$\sum_a \ell_{1j}^{ab} = 0 \tag{12}$$

holds for $j = 1, 2$. If the collision operator possesses the self-adjoint property, it ensures the symmetry of the friction coefficients,

$$\ell_{ij}^{ab} = \ell_{ji}^{ba}. \tag{13}$$

The combination of momentum conservation and the self-adjointness leads to

$$\sum_b \ell_{i1}^{ab} = 0 \tag{14}$$

for $i = 1, 2$. These relations are mentioned in Appendix D of Ref. 22, and their proof is considered straightforward enough to be omitted here.

In an axisymmetric system, the neoclassical viscous forces only damp the magnitude of the poloidal components of the particle and heat flows. They can be expressed as[5,39]

$$\langle \boldsymbol{B}\cdot\nabla\cdot\boldsymbol{\Pi}_a\rangle = 3\langle(\boldsymbol{n}\cdot\nabla B)^2\rangle\left(\mu_{a1}\hat{u}_{a\theta} + \frac{2}{5}\mu_{a2}\frac{\hat{q}_{a\theta}}{p_a}\right), \tag{15}$$

$$\langle \boldsymbol{B}\cdot\nabla\cdot\boldsymbol{\Theta}_a\rangle = 3\langle(\boldsymbol{n}\cdot\nabla B)^2\rangle\left(\mu_{a2}\hat{u}_{a\theta} + \frac{2}{5}\mu_{a3}\frac{\hat{q}_{a\theta}}{p_a}\right), \tag{16}$$

where $\boldsymbol{n} = \boldsymbol{B}/B$ and μ_{ak} for $k = 1, 2, 3$ represent the parallel neoclassical viscosities for species a. The poloidal flow $\hat{u}_{a\theta}$ and the poloidal heat flow $\hat{q}_{a\theta}$ are defined as the flux functions: $\hat{u}_{a\theta} \equiv (\boldsymbol{u}_a\cdot\nabla\theta)/(\boldsymbol{B}\cdot\nabla\theta)$ and $\hat{q}_{a\theta} \equiv (\boldsymbol{q}_a\cdot\nabla\theta)/(\boldsymbol{B}\cdot\nabla\theta)$, respectively. The particle and heat flow velocities are

$$\boldsymbol{u}_a = \boldsymbol{u}_{a\perp} + u_{a\|}\boldsymbol{n}, \tag{17}$$

$$\boldsymbol{q}_a = \boldsymbol{q}_{a\perp} + q_{a\|}\boldsymbol{n}, \tag{18}$$

while the perpendicular flow velocities are the first order classical diamagnetic flows,

$$\boldsymbol{u}_{a\perp} = \frac{\boldsymbol{B}\times\nabla p_a}{e_a n_a B^2} + \frac{\boldsymbol{E}\times\boldsymbol{B}}{B^2}, \tag{19}$$

$$\boldsymbol{q}_{a\perp} = \frac{5}{2}p_a\frac{\boldsymbol{B}\times\nabla T_a}{e_a B^2}. \tag{20}$$

The scalar product of Eqs. (17) and (18) with $\nabla\theta$ yields the parallel flows after taking the flux-surface average,

$$\langle Bu_{a\|}\rangle = BV_{1a} + \hat{u}_{a\theta}\langle B^2\rangle, \tag{21}$$

$$\frac{2\langle Bq_{a\|}\rangle}{5p_a} = BV_{2a} + \frac{2\hat{q}_{a\theta}}{5p_a}\langle B^2\rangle. \tag{22}$$

The diamagnetic flows BV_{1a} and BV_{2a} are naturally determined as

$$BV_{1a} = -I\frac{T_a}{e_a}\frac{\partial \ln p_a}{\partial\psi} - I\frac{\partial\Phi}{\partial\psi}, \tag{23}$$

$$BV_{2a} = -I\frac{T_a}{e_a}\frac{\partial \ln T_a}{\partial\psi}, \tag{24}$$

where Φ is the electrostatic potential. The spatial gradient of Φ corresponds to E_r through $E_r \approx -\partial_\psi\Phi$. We note that BV_{1a} and BV_{2a} are flux functions. The viscous coefficient of $\hat{q}_{a\theta}$ in Eq. (15), i.e., μ_{a2}, and that of $\hat{u}_{a\theta}$ in Eq. (16) are the same due to the self-adjoint property of the collision operator.[5]

B. Banana-plateau fluxes

In the long mean free path regime, the primary force balances in the momentum and heat flux equations parallel to the magnetic field occur between the viscosity forces and the friction forces,

$$\langle \boldsymbol{B}\cdot\nabla\cdot\boldsymbol{\Pi}_a\rangle = \langle BF_{a1\|} + e_a n_a BE_\|\rangle, \tag{25}$$

$$\langle \boldsymbol{B}\cdot\nabla\cdot\boldsymbol{\Theta}_a\rangle = \langle BF_{a2\|}\rangle, \tag{26}$$

where $\boldsymbol{\Pi}$ and $\boldsymbol{\Theta}$ are the viscous stress tensor and the viscous heat stress tensor, respectively.

Ambipolarity of the banana-plateau flux can be straightforwardly verified without explicitly knowing the expressions of the flows. From Eqs. (8) and (10), we obtain

$$
\begin{aligned}
&\sum_a e_a \langle \boldsymbol{\Gamma}_a^{\mathrm{BP}} \cdot \nabla\psi \rangle \\
&= -\frac{I}{\langle B^2 \rangle} \sum_a \langle \boldsymbol{B} \cdot \nabla \cdot \boldsymbol{\Pi}_a \rangle \\
&= -\frac{I}{\langle B^2 \rangle} \sum_a \langle BF_{a1\|} + e_a n_a BE_\| \rangle \\
&= -\frac{I}{\langle B^2 \rangle} \sum_b \left[\left(\sum_a \ell_{11}^{ab} \right) \langle Bu_{b\|} \rangle - \left(\sum_a \ell_{12}^{ab} \right) \frac{2\langle Bq_{b\|} \rangle}{5p_b} \right] \\
&\quad - \frac{1}{\langle B^2 \rangle} \left(\sum_a e_a n_a \right) \langle BE_\| \rangle \\
&= 0.
\end{aligned} \tag{27}
$$

It is evident that ambipolarity is established solely through momentum conservation given in Eq. (12) and quasi-neutrality, regardless of the particle and heat flows, as noted in Refs. 5 and 38. Although theoretical proof of ambipolarity was sufficient in Eq. (27), it was necessary to confirm its validity through the same process actually calculated in numerical codes such as MI[6,23,24] and NCLASS.[7] Both codes calculate the neoclassical flows and subsequently the fluxes by numerically inverting the matrix consisting of friction coefficients and viscosities, solving the simultaneous equations. In the references of both codes, there is no mention of ambipolarity, or if there is, there is no analytical discussion of the necessary conditions for ambipolarity to hold.

Another important feature in an axisymmetric system, namely, the independence of the poloidal flow and the particle flux from E_r, is not mentioned either. Hirshman[5,39] analytically derived this feature based on the assumption that the viscous forces are smaller than the friction forces: $\Delta_a \equiv \mathrm{Max}(\Delta_{ij}^a)$, where $\Delta_{ij}^a \equiv (3\langle(\boldsymbol{n}\cdot\nabla B)^2\rangle/\langle B^2\rangle)(\mu_{ai}/\ell_{ij}^{aa}) < 1$. This assumption directly implies the negligible contribution of the viscous forces in the left-hand side of Eqs. (25) and (26). To $\mathscr{O}(\Delta_a)$, neglecting the parallel electric field, momentum conservation given in Eq. (12) leads to the existence of a common parallel flow, where all parallel particle flows have the same value, and simultaneously the absence of a common parallel heat flow. By introducing the common parallel flow, which can be derived from $\sum_a \langle \boldsymbol{B}\cdot\nabla\cdot\boldsymbol{\Pi}_a\rangle = 0$, into Eq. (21), it is found that $\hat{u}_{a\theta}$ is independent of $\partial_\psi \Phi$. The detailed derivation of this fact is given in Appendix. However, this conclusion was reached under the specific assumption of virtually ignored viscous forces, and it is not clear whether the same conclusion can be reached when these forces are explicitly considered. Furthermore, besides momentum conservation, it is unknown whether other conditions, such as the self-adjointness, are required. Therefore, it is of significant importance to clarify these analytically in a more general situation.

Up to this point, particle species have been represented using the symbols a and b. For convenience in the following matrix calculations, we will replace the symbols representing particle species with numbers. For instance, if the plasma consists of electrons, main ions, and one impurity ion, they will correspond to 1, 2, and 3, respectively, and the total number of species n will be 3. Let us define the sets $M = \{1, 2, \ldots, n\}$ and $N = \{1, 2, \ldots, n, n+1, n+2, \ldots, 2n\}$.

By substituting Eqs. (21) and (22) into a set of equations obtained by substituting Eqs. (15) and (16) into Eqs. (25) and (26), we express the parallel particle and heat flows for species i without the poloidal flows,

$$
\begin{aligned}
\begin{bmatrix} \langle Bu_{i\|} \rangle \\ \dfrac{2\langle Bq_{i\|} \rangle}{5p_i} \end{bmatrix} &= -\sum_{j=1}^{n} \begin{bmatrix} (c_{i,j}) & (c_{i,n+j}) \\ (c_{n+i,j}) & (c_{n+i,n+j}) \end{bmatrix} \begin{bmatrix} BV_{1j} \\ BV_{2j} \end{bmatrix} \\
&\quad -\sum_{j=1}^{n} \begin{bmatrix} (b_{i,j}) & (b_{i,n+j}) \\ (b_{n+i,j}) & (b_{n+i,n+j}) \end{bmatrix} \begin{bmatrix} e_j n_j \langle BE_\| \rangle \\ 0 \end{bmatrix},
\end{aligned} \tag{28}
$$

where $(c_{i,j})$ and $(b_{i,j})$ for $i, j \in M$ are abbreviated notations for the matrices, which are submatrices of $\mathbf{C}$ and $\mathbf{B}$, respectively. Hereafter, unless otherwise specified, the subscripts i and j range from 1 to n when a matrix is written in this form. We will scrutinize what $(c_{i,j})$ and $(b_{i,j})$ actually represent. First, we observe that the viscous matrix $\mathbf{D}$ becomes a block diagonal matrix since the viscosity tensor of species a in Eqs. (15) and (16) depends only on the flows and viscosity coefficients of species a. Therefore, $\mathbf{D}$ can be expressed as

$$
\mathbf{D} = \begin{bmatrix} \mathrm{diag}(d_{1,1}, \ldots, d_{n,n}) & \mathrm{diag}(d_{1,n+1}, \ldots, d_{n,2n}) \\ \mathrm{diag}(d_{n+1,1}, \ldots, d_{2n,n}) & \mathrm{diag}(d_{n+1,n+1}, \ldots, d_{2n,2n}) \end{bmatrix}, \tag{29}
$$

where, for $i \in M$,

$$
d_{i,i} = \tilde{\mu}_{i,1}, \quad d_{i,n+i} = d_{n+i,i} = \tilde{\mu}_{i,2},\ d_{n+i,n+i} = \tilde{\mu}_{i,3} \tag{30}
$$

and

$$
\tilde{\mu}_{ik} \equiv (-1)^{k+1} \frac{3\langle(\boldsymbol{n}\cdot\nabla B)^2\rangle}{\langle B^2\rangle} \mu_{ik}. \quad k = 1, 2, 3. \tag{31}
$$

The self-adjointness of the collision operator ensures the symmetric property of $\mathbf{D}$, i.e., $d_{i,n+i} = d_{n+i,i}$. By defining $\tilde{\mu}_{ik}$ as in Eq. (31), which includes $(-1)^{k+1}$, we can express the friction coefficient matrix as

$$
\mathbf{L} = \begin{bmatrix} (\ell_{11}^{ij}) & (\ell_{12}^{ij}) \\ (\ell_{21}^{ij}) & (\ell_{22}^{ij}) \end{bmatrix} \equiv (l_{i,j})_{i,j\in N}, \tag{32}
$$

such that the minus sign in ℓ^{ij} appearing when $(i+j)$ is odd, as observed in Eqs. (10) and (11), is eliminated. We then define the matrix $\mathbf{A}$ as $\mathbf{A} \equiv \mathbf{L} - \mathbf{D}$ and its inverse matrix as $\mathbf{B} \equiv \mathbf{A}^{-1}$. Furthermore, we define the matrix product of $\mathbf{BD}$ as $\mathbf{C}$: $\mathbf{C} \equiv \mathbf{BD}$. It is now evident that $(c_{ij})_{i,j\in N} = \mathbf{C}$ and $(b_{ij})_{i,j\in N} = \mathbf{B}$.

Now that the parallel flows can be explicitly described, the poloidal flows can be expressed as follows using Eqs. (21) and (22):

$$
\begin{aligned}
\begin{bmatrix} \hat{u}_{i\theta} \\ \dfrac{2\hat{q}_{i\theta}}{5p_i} \end{bmatrix} &= -\frac{1}{\langle B^2\rangle} \sum_{j=1}^{n} \begin{bmatrix} (c_{i,j}) + \delta_{i,j} & (c_{i,n+j}) \\ (c_{n+i,j}) & (c_{n+i,n+j}) + \delta_{i,j} \end{bmatrix} \begin{bmatrix} BV_{1j} \\ BV_{2j} \end{bmatrix} \\
&\quad -\frac{1}{\langle B^2\rangle} \sum_{j=1}^{n} \begin{bmatrix} (b_{i,j}) & (b_{i,n+j}) \\ (b_{n+i,j}) & (b_{n+i,n+j}) \end{bmatrix} \begin{bmatrix} e_j n_j \langle BE_\| \rangle \\ 0 \end{bmatrix},
\end{aligned} \tag{33}
$$

where $\delta_{i,j}$ is the Kronecker delta, which equals one when $i = j$ and zero otherwise. These equations are exactly the algebraic equations solved in MI.[6] Since the expressions of the friction forces, which are independent of the magnetic field, are valid in all collisionality regimes, the expressions of the poloidal flows are also valid in all regimes when the viscous force expressions applicable among the various regimes are adopted. It is evident from Eq. (23) that the diamagnetic flow explicitly contains the term $\partial_\psi \Phi$, representing E_r. However, in an axisymmetric system, the poloidal flows are found to be independent of $\partial_\psi \Phi$.[5] This implies that to this order, the toroidal flows can be arbitrary due to the axisymmetry and the conservation of the toroidal angular momentum. In combination with Eqs. (23), (24), and (33), we observe that the following conditions must be satisfied for any $i \in M$:

$$\sum_{j=1}^{n}\left[c_{i,j} + \delta_{i,j}\right] = 0, \quad \text{or equivalently,} \quad \sum_{j=1}^{n} c_{i,j} = -1, \tag{34}$$

$$\sum_{j=1}^{n} c_{n+i,j} = 0. \tag{35}$$

Here, $c_{i,j}$ denotes the (i, j) entry of the matrix $\mathbf{C}$. For the time being, we will proceed assuming that the above conditions are satisfied. In Sec. II C, we will revisit this issue to thoroughly examine the algebraic conditions under which the aforementioned equations hold.

We define the thermodynamic forces A_1^i and A_2^i and the parallel electric field force A_3^i as follows:

$$A_1^i = \frac{\partial \ln p_i}{\partial \psi}, \tag{36}$$

$$A_2^i = \frac{\partial \ln T_i}{\partial \psi}, \tag{37}$$

$$A_3^i = e_i \frac{\langle B E_\| \rangle}{\langle B^2 \rangle}. \tag{38}$$

If Eqs. (34) and (35) are satisfied, the term involving the electrostatic potential in Eq. (33) vanishes in the expressions of the poloidal flows.

Now we observe that the particle and heat fluxes in the banana-plateau regime given in Eqs. (8) and (9) can be expressed in terms of the poloidal flows, $\hat{u}_{i\theta}$ and $2\hat{q}_{i\theta}/(5p_i)$, using Eq. (33). By substituting Eq. (33) into the fluxes in the banana-plateau regime, we can represent these fluxes in terms of the thermodynamic forces A_1^i and A_2^i and the parallel electric field force A_3^i. Similarly, the parallel current $e_k n_k \langle B u_{k\|} \rangle$ can be expressed using Eq. (28). As a result, the cross field fluxes and the parallel current can be expressed in the matrix form (c.f. Ref. 38) as follows:

$$\begin{bmatrix} \langle \boldsymbol{\Gamma}_i^{\mathrm{BP}} \cdot \nabla\psi \rangle \\ T_i^{-1} \langle \boldsymbol{q}_i^{\mathrm{BP}} \cdot \nabla\psi \rangle \\ e_i n_i \langle B u_{i\|} \rangle \end{bmatrix} = \sum_{j=1}^{n} \begin{bmatrix} L_{11}^{ij} & L_{12}^{ij} & L_{13}^{ij} \\ L_{21}^{ij} & L_{22}^{ij} & L_{23}^{ij} \\ L_{31}^{ij} & L_{32}^{ij} & L_{33}^{ij} \end{bmatrix} \begin{bmatrix} A_1^j \\ A_2^j \\ A_3^j \end{bmatrix}. \tag{39}$$

Here, the matrix components L are given as follows:

$$L_{11}^{ij} = -\frac{I^2}{\langle B^2 \rangle} \frac{T_j}{e_i e_j} \left[d_{i,i}(\delta_{i,j} + c_{i,j}) + d_{i,n+i} c_{n+i,j} \right], \tag{40}$$

$$L_{12}^{ij} = -\frac{I^2}{\langle B^2 \rangle} \frac{T_j}{e_i e_j} \left[d_{i,i} c_{i,n+j} + d_{i,n+i}(\delta_{i,j} + c_{n+i,n+j}) \right], \tag{41}$$

$$L_{21}^{ij} = -\frac{I^2}{\langle B^2 \rangle} \frac{T_j}{e_i e_j} \left[d_{n+i,i}(\delta_{i,j} + c_{i,j}) + d_{n+i,n+i} c_{n+i,j} \right], \tag{42}$$

$$L_{22}^{ij} = -\frac{I^2}{\langle B^2 \rangle} \frac{T_j}{e_i e_j} \left[d_{n+i,i} c_{i,n+j} + d_{n+i,n+i}(\delta_{i,j} + c_{n+i,n+j}) \right], \tag{43}$$

$$L_{13}^{ij} = I \frac{n_j}{e_i} \left[d_{i,i} b_{i,j} + d_{i,n+i} b_{n+i,j} \right], \tag{44}$$

$$L_{23}^{ij} = I \frac{n_j}{e_i} \left[d_{n+i,i} b_{i,j} + d_{n+i,n+i} b_{n+i,j} \right], \tag{45}$$

$$L_{31}^{ij} = -I \frac{n_i}{e_j} c_{i,j}, \tag{46}$$

$$L_{32}^{ij} = -I \frac{n_i}{e_j} c_{i,n+j}, \tag{47}$$

$$L_{33}^{ij} = -\langle B^2 \rangle e_i e_j n_i n_j b_{i,j}. \tag{48}$$

The sum of the particle fluxes of each species multiplied by their respective charge must be zero in order for ambipolarity to hold,

$$\sum_{i=1}^{n} e_i \langle \boldsymbol{\Gamma}_i^{\mathrm{BP}} \cdot \nabla\psi \rangle = \sum_{j=1}^{n} \left[\left(\sum_{i=1}^{n} e_i L_{11}^{ij} \right) A_1^j + \left(\sum_{i=1}^{n} e_i L_{12}^{ij} \right) A_2^j \right] + \left(\sum_{i=1}^{n} \sum_{j=1}^{n} e_i e_j L_{13}^{ij} \right) \frac{\langle B E_\| \rangle}{\langle B^2 \rangle} = 0. \tag{49}$$

Therefore, for any $j \in M$, the following conditions must be satisfied simultaneously:

$$\sum_{i=1}^{n} e_i L_{11}^{ij} = 0, \tag{50}$$

$$\sum_{i=1}^{n} e_i L_{12}^{ij} = 0, \tag{51}$$

$$\sum_{i=1}^{n} \sum_{j=1}^{n} e_i e_j L_{13}^{ij} = 0. \tag{52}$$

C. Necessary conditions for ambipolarity of the banana-plateau flux

We have examined the necessary conditions for ambipolarity in detail. We have revealed that Eqs. (50)–(52) must all be satisfied for ambipolarity to hold. In this section, we employ linear algebra to elucidate the essential physical conditions required for ambipolarity. While Eqs. (34) and (35) are not strictly necessary for ambipolarity, they do play a crucial role in ensuring that the poloidal flows, and consequently the particle fluxes, remain independent of E_r in an axisymmetric system.

First, we focus on the necessary conditions for Eqs. (34) and (35). The matrix $\mathbf{C} = \mathbf{BD}$ can be expressed as

$$\mathbf{C} = \begin{bmatrix} (c_{i,j}) & (c_{i,n+j}) \\ (c_{n+i,j}) & (c_{n+i,n+j}) \end{bmatrix} = \begin{bmatrix} (b_{i,j} d_{j,j} + b_{i,n+j} d_{n+j,j}) & (b_{i,j} d_{j,n+j} + b_{i,n+j} d_{n+j,n+j}) \\ (b_{n+i,j} d_{j,j} + b_{n+i,n+j} d_{n+j,j}) & (b_{n+i,j} d_{j,n+j} + b_{n+i,n+j} d_{n+j,n+j}) \end{bmatrix}, \tag{53}$$

by applying Eq. (29). Since the matrix $\mathbf{B}$ is the inverse of the matrix $\mathbf{A}$, the (i, j) entry of $\mathbf{B}$ can be written as

$$b_{i,j} = \frac{1}{|\mathbf{A}|} \tilde{a}_{j,i}, \tag{54}$$

where $|\mathbf{A}|$ represents the determinant of $\mathbf{A}$, and $\tilde{a}_{j,i}$ represents the cofactor of $A_{j,i}$ in $\mathbf{A}$. The determinant of a square matrix can be expanded along an arbitrary row or column number using the cofactors. This is called the Laplace expansion or the cofactor expansion. For this case, the $2n$-order square matrix $\mathbf{A}$ can be expanded as

$$|\mathbf{A}| = \sum_{k=1}^{2n} a_{i,k}\tilde{a}_{i,k} = \sum_{k=1}^{2n} a_{k,j}\tilde{a}_{k,j}. \tag{55}$$

An important feature of the Laplace expansion is that when $i \neq j$, we have

$$0 = \sum_{k=1}^{2n} a_{i,k}\tilde{a}_{j,k} = \sum_{k=1}^{2n} a_{k,i}\tilde{a}_{k,j}. \tag{56}$$

We now recall that $\mathbf{A} = \mathbf{L} - \mathbf{D}$, where $\mathbf{L}$ and $\mathbf{D}$ are the matrices of the friction coefficients and the viscosities, respectively. It is apparent that momentum conservation given in Eq. (12), which can now be rewritten as $\sum_{i=1}^{n} l_{i,j} = 0$ for any $j \in N$, solely derives

$$\sum_{i=1}^{n} a_{i,j} = \sum_{i=1}^{n} l_{i,j} - \sum_{i=1}^{n} d_{i,j} = -d_{j,j}, \tag{57}$$

and similarly,

$$\sum_{i=1}^{n} a_{i,n+j} = -d_{j,n+j} \tag{58}$$

for any $j \in M$. Assuming the self-adjointness in addition to momentum conservation, Eq. (14) holds, which can be rewritten as $\sum_{j=1}^{n} l_{i,j} = 0$ for any $i \in N$, and we obtain

$$\sum_{j=1}^{n} a_{i,j} = \sum_{j=1}^{n} l_{i,j} - \sum_{j=1}^{n} d_{i,j} = -d_{i,i}, \tag{59}$$

and similarly,

$$\sum_{j=1}^{n} a_{n+i,j} = -d_{n+i,j} \tag{60}$$

for any $i \in M$. We note that the symmetric property of $d_{i,n+i} = d_{n+i,j}$ in Eq. (30), stemming from Eqs. (15) and (16), is the consequence of the self-adjointness of the collision operator used to derive viscosities. With this symmetry, another symmetric property of the friction coefficients as a consequence of the self-adjointness shown in Eq. (13), i.e., $l_{i,j} = l_{j,i}$, leads to

$$a_{i,j} = a_{j,i}. \tag{61}$$

We first examine the necessary conditions for Eq. (34) to hold,

$$\begin{aligned}
\sum_{j=1}^{n} c_{i,j} &= \sum_{j=1}^{n} \left[b_{i,j}d_{j,j} + b_{i,n+j}d_{n+j,j} \right], \\
&= -\frac{1}{|\mathbf{A}|}\sum_{j=1}^{n}\left[\tilde{a}_{j,i}\sum_{k=1}^{n} a_{k,j} + \tilde{a}_{n+j,i}\sum_{k=1}^{n} a_{n+j,k} \right], \\
&= -\frac{1}{|\mathbf{A}|}\sum_{j=1}^{n}\left[\tilde{a}_{j,i}\sum_{k=1}^{n} a_{j,k} + \tilde{a}_{n+j,i}\sum_{k=1}^{n} a_{n+j,k} \right], \\
&= -\frac{1}{|\mathbf{A}|}\left[\sum_{k=1}^{2n}\tilde{a}_{k,i}a_{k,i} + \sum_{l=1,l\neq j}^{n}\sum_{k=1}^{2n}\tilde{a}_{k,i}a_{k,l} \right], \\
&= -\frac{1}{|\mathbf{A}|}\left[|\mathbf{A}| + 0 \right] = -1.
\end{aligned} \tag{62}$$

The second equality follows from Eqs. (57) and (60), which mean that both momentum conservation and the self-adjointness are required. The third equality follows from the self-adjointness, shown in Eq. (61). Equations (55) and (56) have been applied in the second-to-last equality. Similarly, for Eq. (35),

$$\begin{aligned}
\sum_{j=1}^{n} c_{n+i,j} &= \sum_{j=1}^{n} \left[b_{n+i,j}d_{j,j} + b_{n+i,n+j}d_{n+j,j} \right], \\
&= -\frac{1}{|\mathbf{A}|}\sum_{j=1}^{n}\left[\tilde{a}_{j,n+i}\sum_{k=1}^{n} a_{k,j} + \tilde{a}_{n+j,n+i}\sum_{k=1}^{n} a_{n+j,k} \right], \\
&= -\frac{1}{|\mathbf{A}|}\sum_{j=1}^{n}\left[\tilde{a}_{j,n+i}\sum_{k=1}^{n} a_{j,k} + \tilde{a}_{n+j,n+i}\sum_{k=1}^{n} a_{n+j,k} \right], \\
&= -\frac{1}{|\mathbf{A}|}\left[\sum_{l=1}^{n}\sum_{k=1}^{2n}\tilde{a}_{k,n+i}a_{k,l} \right], \\
&= 0.
\end{aligned} \tag{63}$$

The linear algebraic calculation has revealed that not only momentum conservation but also *the self-adjointness* must be required to render the poloidal flows independent of the electrostatic potential.

Next, the ambipolarity conditions will be investigated. It has already been found from Eq. (27) that only momentum conservation ensures ambipolarity of the banana-plateau flux, and this fact will be verified in the following algebraic calculation. The left-hand sides of Eqs. (50)–(52) can be written as

$$\sum_{i=1}^{n} e_j L_{11}^{ij} = -\frac{I^2}{\langle B^2\rangle}\frac{T_j}{e_j}\left\{ \sum_{i=1}^{n}\left[d_{i,i}c_{i,j} + d_{i,n+i}c_{n+i,j} \right] + d_{j,j} \right\}, \tag{64}$$

$$\sum_{i=1}^{n} e_j L_{12}^{ij} = -\frac{I^2}{\langle B^2\rangle}\frac{T_j}{e_j}\left\{ \sum_{i=1}^{n}\left[d_{i,i}c_{i,n+j} + d_{i,n+i}c_{n+i,n+j} \right] + d_{j,n+j} \right\}, \tag{65}$$

$$\sum_{i=1}^{n}\sum_{j=1}^{n} e_i e_j L_{13}^{ij} = I\sum_{j=1}^{n} e_j n_j \left\{ \sum_{i=1}^{n}\left[d_{i,i}b_{i,j} + d_{i,n+i}b_{n+i,j} \right] \right\}. \tag{66}$$

For Eqs. (50)–(52) to hold, we should apparently examine the expressions in $\{\cdots\}$. With regard to Eq. (64),

$$\begin{aligned}
&\sum_{i=1}^{n}\left[d_{i,i}c_{i,j} + d_{i,n+i}c_{n+i,j} \right] \\
&= \sum_{i=1}^{n}\left[d_{i,i}(b_{i,j}d_{j,j} + b_{i,n+j}d_{n+j,j}) + d_{i,n+i}(b_{n+i,j}d_{j,j} + b_{n+i,n+j}d_{n+j,j}) \right] \\
&= d_{j,j}\left[\sum_{i=1}^{n}(b_{i,j}d_{i,i} + b_{n+i,j}d_{i,n+i}) \right] \\
&\quad + d_{n+j,j}\left[\sum_{i=1}^{n}(b_{i,n+j}d_{i,i} + b_{n+i,n+j}d_{i,n+i}) \right] \\
&= -\frac{d_{j,j}}{|\mathbf{A}|}\sum_{i=1}^{n}\left[\tilde{a}_{j,i}\sum_{k=1}^{n} a_{k,i} + \tilde{a}_{j,n+i}\sum_{k=1}^{n} a_{k,n+i} \right] \\
&\quad - \frac{d_{n+j,j}}{|\mathbf{A}|}\sum_{i=1}^{n}\left[\tilde{a}_{n+j,i}\sum_{k=1}^{n} a_{k,i} + \tilde{a}_{n+j,n+i}\sum_{k=1}^{n} a_{k,n+i} \right] \\
&= -\frac{d_{j,j}}{|\mathbf{A}|}\left[\sum_{k=1}^{2n}\tilde{a}_{j,k}a_{j,k} + \sum_{l=1,l\neq j}^{n}\sum_{k=1}^{2n}\tilde{a}_{j,k}a_{j,l} \right] - \frac{d_{n+j,j}}{|\mathbf{A}|}\sum_{l=1}^{n}\sum_{k=1}^{2n}\tilde{a}_{n+j,k}a_{l,k} \\
&= -d_{j,j}.
\end{aligned} \tag{67}$$

In the course of the reduction, we have only used Eqs. (57) and (58) to obtain the third equality. Similarly, Eq. (65) can be reduced as

$$\begin{aligned}\sum_{i=1}^{n}&[d_{i,i}c_{i,n+j}+d_{i,n+i}c_{n+i,n+j}]\\ &=\sum_{i=1}^{n}[d_{i,i}(b_{i,j}d_{j,n+j}+b_{i,n+j}d_{n+j,n+j})\\ &\quad+d_{i,n+i}(b_{n+i,j}d_{j,n+j}+b_{n+i,n+j}d_{n+j,n+j})]\\ &=d_{j,n+j}\left[\sum_{i=1}^{n}(b_{i,j}d_{i,i}+b_{n+i,j}d_{i,n+i})\right]\\ &\quad+d_{n+j,n+j}\left[\sum_{i=1}^{n}(b_{i,n+j}d_{i,i}+b_{n+i,n+j}d_{i,n+i})\right]\\ &=-d_{j,n+j}.\end{aligned}\tag{68}$$

The terms in the brackets in the second equality are the same as those in Eq. (67), and the detailed explanation of manipulating the equation after the second equality has not been repeated here. Finally, Eq. (66) turns out to be

$$\begin{aligned}\sum_{i=1}^{n}&[d_{i,i}b_{i,j}+d_{i,n+i}b_{n+i,j}]\\ &=\frac{1}{|\mathbf{A}|}\sum_{i=1}^{n}\left[\tilde{a}_{j,i}\sum_{k=1}^{n}a_{k,i}+\tilde{a}_{j,n+i}\sum_{k=1}^{n}a_{k,n+i}\right]\\ &=-\frac{1}{|\mathbf{A}|}\left[\sum_{k=1}^{2n}\tilde{a}_{j,k}a_{j,k}+\sum_{l=1,l\neq j}^{n}\sum_{k=1}^{2n}\tilde{a}_{j,k}a_{j,l}\right]\\ &=-1.\end{aligned}\tag{69}$$

Again, momentum conservation has been solely used here.

Equations (67)–(69) are substituted into Eqs. (64)–(66), resulting in the validity of Eqs. (50)–(52). We note that only for Eq. (52) to hold, quasi-neutrality must be additionally required, as apparent from Eqs. (66) and (69). In summary, ambipolarity requires momentum conservation only, and quasi-neutrality is needed as well when $E_\parallel$ exists.

While proving ambipolarity, the assumption has already been made that the poloidal flow is independent of the electrostatic potential, which is equivalent to Eqs. (34) and (35) holding. However, we note that this condition is not necessary for ambipolarity to hold. The thermodynamic force A_1^i given in Eq. (36) could be written as $A_1^i=\partial_\psi \ln p_i+(e_i/T_i)\partial_\psi\Phi$ if the dependence of the electrostatic potential were left explicitly. In this case, ambipolarity additionally requires

$$\sum_{i=1} e_i L_{11}^{ij}\frac{e_j}{T_j}=0,\tag{70}$$

and obviously, it must hold whenever Eq. (64) becomes zero. This feature is referred to as automatic or intrinsic ambipolarity, which means that ambipolarity holds regardless of the value of the electrostatic potential.[5] Through linear algebraic calculations concerning ambipolarity, we have confirmed that the self-adjointness has no influence on ambipolarity, and momentum conservation solely matters in conjunction with quasi-neutrality.

D. Pfirsch–Schlüter and classical fluxes

In the regimes where collisions predominate, the viscosities do not play a significant role, and the fluxes are determined by the friction forces. From Eqs. (8) and (9), the fluxes can be expressed as

$$\begin{bmatrix}\langle\boldsymbol{\Gamma}_a^{\rm PS}\cdot\nabla\psi\rangle\\ T_a^{-1}\langle\boldsymbol{q}_a^{\rm PS}\cdot\nabla\psi\rangle\end{bmatrix}=-\frac{I}{e_a}\left\langle\left(\frac{1}{B^2}-\frac{1}{\langle B^2\rangle}\right)\begin{bmatrix}BF_{a1\parallel}\\ BF_{a2\parallel}\end{bmatrix}\right\rangle.\tag{71}$$

By substituting the friction forces given in Eqs. (10) and (11), as well as the parallel flows given in Eqs. (21) and (22), we obtain the particle and heat fluxes for species a in the Pfirsch–Schlüter regime as

$$\begin{aligned}&\begin{bmatrix}\langle\boldsymbol{\Gamma}_a^{\rm PS}\cdot\nabla\psi\rangle\\ T_a^{-1}\langle\boldsymbol{q}_a^{\rm PS}\cdot\nabla\psi\rangle\end{bmatrix}\\ &=-\frac{I}{e_a}\left(\left\langle\frac{1}{B^2}\right\rangle-\frac{1}{\langle B^2\rangle}\right)\sum_b\begin{bmatrix}\ell_{11}^{ab} & -\ell_{12}^{ab}\\ -\ell_{21}^{ab} & \ell_{22}^{ab}\end{bmatrix}\begin{bmatrix}BV_{1b}\\ BV_{2b}\end{bmatrix}\\ &=\frac{I^2}{e_a}\left(\left\langle\frac{1}{B^2}\right\rangle-\frac{1}{\langle B^2\rangle}\right)\sum_b\frac{T_b}{e_b}\begin{bmatrix}\ell_{11}^{ab} & -\ell_{12}^{ab}\\ -\ell_{21}^{ab} & \ell_{22}^{ab}\end{bmatrix}\begin{bmatrix}\dfrac{\partial\ln p_b}{\partial\psi}+\dfrac{e_b}{T_b}\dfrac{\partial\Phi}{\partial\psi}\\ \dfrac{\partial\ln T_b}{\partial\psi}\end{bmatrix}.\end{aligned}\tag{72}$$

In the process of derivation, the relation $\langle(B^{-2}-\langle B^2\rangle^{-1})B^2\rangle=0$ was applied, which eliminated the dependence of the fluxes on the poloidal flows. It is evident that negating $\partial_\psi\Phi$ in the fluxes requires $\sum_b \ell_{i1}^{ab}=0$ for $i=1$, 2, which is identical to Eq. (14). This fact indicates that both momentum conservation and the self-adjointness are necessary, similar to the case of the banana-plateau fluxes.

Next, it can be readily found that

$$\begin{aligned}\sum_a e_a\langle\boldsymbol{\Gamma}_a^{\rm PS}\cdot\nabla\psi\rangle&=I^2\left(\left\langle\frac{1}{B^2}\right\rangle-\frac{1}{\langle B^2\rangle}\right)\\ &\quad\times\sum_b\left[\left(\sum_a\ell_{11}^{ab}\right)\left(\frac{T_b}{e_b}\frac{\partial\ln p_b}{\partial\psi}+\frac{\partial\Phi}{\partial\psi}\right)\right.\\ &\quad\left.-\left(\sum_a\ell_{12}^{ab}\right)\frac{T_b}{e_b}\frac{\partial\ln T_b}{\partial\psi}\right]\end{aligned}\tag{73}$$

would be zero when $\sum_a\ell_{1j}^{ab}=0$ for $j=1$, 2, which corresponds to momentum conservation as shown in Eq. (12). Finally, similar to the banana-plateau flux, ambipolarity is satisfied through momentum conservation alone.

Next, let us examine the classical fluxes. From Eqs. (8) and (9), they can be expressed as

$$\begin{bmatrix}\langle\boldsymbol{\Gamma}_a^{\rm CL}\cdot\nabla\psi\rangle\\ T_a^{-1}\langle\boldsymbol{q}_a^{\rm CL}\cdot\nabla\psi\rangle\end{bmatrix}=\frac{1}{e_a}\left\langle\frac{1}{B^2}\begin{bmatrix}\boldsymbol{B}\times\nabla\psi\cdot\boldsymbol{F}_{a1}\\ \boldsymbol{B}\times\nabla\psi\cdot\boldsymbol{F}_{a2}\end{bmatrix}\right\rangle.\tag{74}$$

We will now substitute Eqs. (10) and (11) into the expressions. Recalling $\boldsymbol{B}\cdot\nabla\psi=0$ if nested flux surfaces exist, we can confirm

$$\begin{aligned}\boldsymbol{B}\times\nabla\psi\cdot\boldsymbol{u}_a&=-\boldsymbol{B}\times\boldsymbol{u}_{a\perp}\cdot\nabla\psi\\ &=-|\nabla\psi|^2\frac{T_a}{e_a}\left(\frac{\partial\ln p_a}{\partial\psi}+\frac{e_a}{T_a}\frac{\partial\Phi}{\partial\psi}\right).\end{aligned}\tag{75}$$

Here, we have applied Eqs. (17) and (19). Similarly, we have

$$\frac{2}{5}\frac{\boldsymbol{B}\times\nabla\psi\cdot\boldsymbol{q}_a}{p_a} = -|\nabla\psi|^2\frac{T_a}{e_a}\frac{\partial\ln T_a}{\partial\psi}. \tag{76}$$

From these, we obtain

$$\begin{bmatrix}\langle\boldsymbol{\Gamma}_a^{\mathrm{CL}}\cdot\nabla\psi\rangle \\ T_a^{-1}\langle\boldsymbol{q}_a^{\mathrm{CL}}\cdot\nabla\psi\rangle\end{bmatrix} = \frac{1}{e_a}\left\langle\frac{|\nabla\psi|^2}{B^2}\right\rangle\sum_b\frac{T_b}{e_b}\begin{bmatrix}\ell_{11}^{ab} & -\ell_{12}^{ab} \\ -\ell_{21}^{ab} & \ell_{22}^{ab}\end{bmatrix} \times\begin{bmatrix}\dfrac{\partial\ln p_b}{\partial\psi}+\dfrac{e_b}{T_b}\dfrac{\partial\Phi}{\partial\psi} \\ \dfrac{\partial\ln T_b}{\partial\psi}\end{bmatrix}. \tag{77}$$

Therefore, the conclusions regarding the independence from $\partial_\psi\Phi$ and ambipolarity for the classical particle fluxes are the same as those for the Pfirsch–Schlüter fluxes since the expressions of the classical fluxes are essentially equivalent to those of the Pfirsch–Schlüter fluxes given in Eq. (72) except for the factors related to the magnetic field. The difference in the factors indicates that the classical fluxes are by one order of the inverse aspect ratio smaller than the Pfirsch–Schlüter fluxes.

E. Self-adjointness

The results obtained in Sec. II can be summarized as follows: Detailed linear algebraic calculations have revealed that the banana-plateau particle flux, Pfirsch–Schlüter flux, and classical flux become independently ambipolar solely due to momentum conservation in the collision operator, and the self-adjointness is not necessarily required for ambipolarity. This characteristic of the classical and neoclassical particle fluxes is known as the detailed balance principle.[5]

In contrast, it is important to note that when using friction coefficients derived from a collision operator that does not satisfy the self-adjointness, the poloidal flows become dependent on E_r. Fortunately, it is known that the fluxes are independent of E_r regardless of the self-adjointness. Therefore, if the poloidal flows given in Eq. (33) are numerically modeled using A_1^i, A_2^i, and A_3^i and explicitly excluding the $\partial_\psi\Phi$ term from the diamagnetic flow BV_{1j}, it is possible to use the friction coefficients that do not satisfy the self-adjointness without violating important physics constraints.

III. IMPURITY EXTENSION OF TASK/TX

Let us begin by providing a brief overview of the major characteristics of TASK/TX. As mentioned in Sec. I, TASK/TX is a one-dimensional fluid-based transport code conforming to the axisymmetric flux coordinates.[37] The governing equations are essentially derived based on a drift-ordered two-fluid model. The electromagnetic fields in a plasma are described by Gauss's law, Faraday's law, and Ampère's law in the code. The time evolution of the plasma as a fluid is governed by a set of differential equations, including the continuity equation, the moment equations in the radial, parallel to the magnetic field and toroidal directions, the heat transport equation, and the parallel heat momentum equation. In addition, two algebraic equations are solved in conjunction with the differential equations, one ensuring the first-order incompressible flow within the flux surface and the other determining the diamagnetic flow as defined in Eq. (23). These equations are solved for each species. While in a physical sense, it is not necessary to separate the algebraic equation for the diamagnetic flow from the radial momentum equation, it has been empirically found that dealing with it separately improves numerical stability with respect to E_r. Furthermore, multiple equations for fast ions and neutrals are incorporated within the framework. This formulation naturally incorporates neoclassical particle transport, the bootstrap current, and resistivity without the need for implementing corresponding terms and coefficients estimated by external neoclassical transport modules. However, it is important to note that within TASK/TX, it is not possible to isolate and extract only the neoclassical contribution from the particle flux,[37] as can be done in conventional transport code frameworks. The particle fluxes in TASK/TX are expressed as the sum of all contributions, including turbulence, neoclassical transport, and sources, and cannot be decomposed into individual components. When observing the neoclassical particle flux alone, after the forces driving turbulent transport are artificially turned off, the simulation is run for a very short duration. The resulting particle fluxes obtained under these conditions represent the neoclassical fluxes, although they still include some other effects like sources, which are usually minor in the core region. For more details on the TASK/TX modeling, please refer to Refs. 36 and 37.

TASK/TX solves nearly identical set of equations for electrons and ions. The equations for each species exhibit minimal differences, with variations occurring only in the coefficients that depend on mass and charge. In the previous work,[37] TASK/TX was limited to handling electrons and hydrogen isotope ions, primarily deuterium, while impurities were not considered. For the purpose of this study, TASK/TX will be extended to incorporate impurity species. The extension of TASK/TX to handle impurities is relatively straightforward since the equations for impurities are very similar to those for the main ions. The main differences arise in the modeling of friction forces and equipartition processes, which are associated with collisions between unlike-particle species. With the inclusion of impurities, the total number of equations to be simultaneously solved increases from 33 to 41.

In this study, fully ionized carbon (C^{6+}) is assumed as the impurity species. Carbon is a commonly observed impurity species in many plasma experiments, and in high-temperature plasmas, it becomes completely ionized within a short time period. However, it should be noted that the modeling of source terms that supply C^{6+} to the core plasma and sink terms that cause its loss from the plasma have not been implemented in the version of TASK/TX used for this study. These aspects will be reported in a separate paper, focusing on the modeling of impurity sources and sinks.

IV. NUMERICAL RESULTS

A. Benchmark tests

A benchmark test was conducted to compare the neoclassical particle fluxes calculated by TASK/TX and MI. As mentioned earlier, the set of governing equations in TASK/TX includes the equations required for neoclassical transport calculations, which were implemented in MI. In this benchmark test, MI was integrated in TASK/TX as a subroutine to compare fluxes under identical conditions, utilizing the exact same plasma profiles. However, it should be emphasized again that TASK/TX is capable of independently calculating neoclassical fluxes alone without MI.

A TASK/TX simulation was performed assuming an L-mode plasma to generate plasma profiles for the purpose of comparison. The circular equilibrium was numerically constructed with a major radius $R = 3.2\,\mathrm{m}$, a minor radius $a = 0.8\,\mathrm{m}$, a plasma current $I_\mathrm{p} = 1\,\mathrm{MA}$, and a toroidal magnetic field $RB_t = 8.576\,\mathrm{Tm}$, and the equilibrium remained unchanged throughout the simulation. The plasma consisted of electrons (e), deuteriums (i), and fully stripped carbon impurities (C). Based on the fact that the exact linearized collision operator does not maintain the self-adjoint property for different mass and temperature ratios between species, it is advisable to setup a situation where the electron-to-ion temperature ratio is large for testing purpose. Therefore, no auxiliary heating was applied, and the electrons were primarily heated by Ohmic heating, as depicted in Fig. 1(b). The presence of Ohmic current and Ohmic heating naturally gives rise to a finite $E_\parallel$, as illustrated in Fig. 1(d). Figure 1(c) demonstrates that carbon experiences higher collisionality compared to electrons and ions due to their larger mass and charge, placing carbon in a different collisionality regime. Particle transport is individually calculated for each species, and the density profiles depicted in Fig. 1(a) are determined based on their respective transport. E_r is formed to be compatible with the slight imbalance in the charge densities in the code. Consequently, the profile of the effective charge number Z_eff is typically nonuniform, as shown in Fig. 1(d).

The expressions of the particle fluxes implemented in MI explicitly incorporate terms associated with $\partial_\psi \Phi$. If a user selects a collision operator model that satisfies the self-adjointness, these terms will have no impact on the fluxes. However, when a user opts for a model that does not precisely satisfy the self-adjointness, these terms will generate fluxes, typically of minor magnitude. In this benchmark test, as MI embedded in TASK/TX is used, it naturally shares $\partial_\psi \Phi$ calculated in TASK/TX in common.

The simulation employed expressions for the friction coefficients that incorporate the effects of higher-order flows.[24] However, as alluded to earlier, it should be noted that the forms of the friction forces remain the same as in Eqs. (10) and (11). The only modification arising from the higher-order flow effects is the replacement of ℓ_{ij}^{ab} with f_{ij}^{ab}, as defined in Ref. 24. If ℓ satisfies Eqs. (12)–(14), f also satisfies them, and vice versa. The conclusions derived in Sec. II therefore remain unchanged, and henceforth, the friction coefficients continue to be denoted as ℓ without distinguishing between ℓ and f.

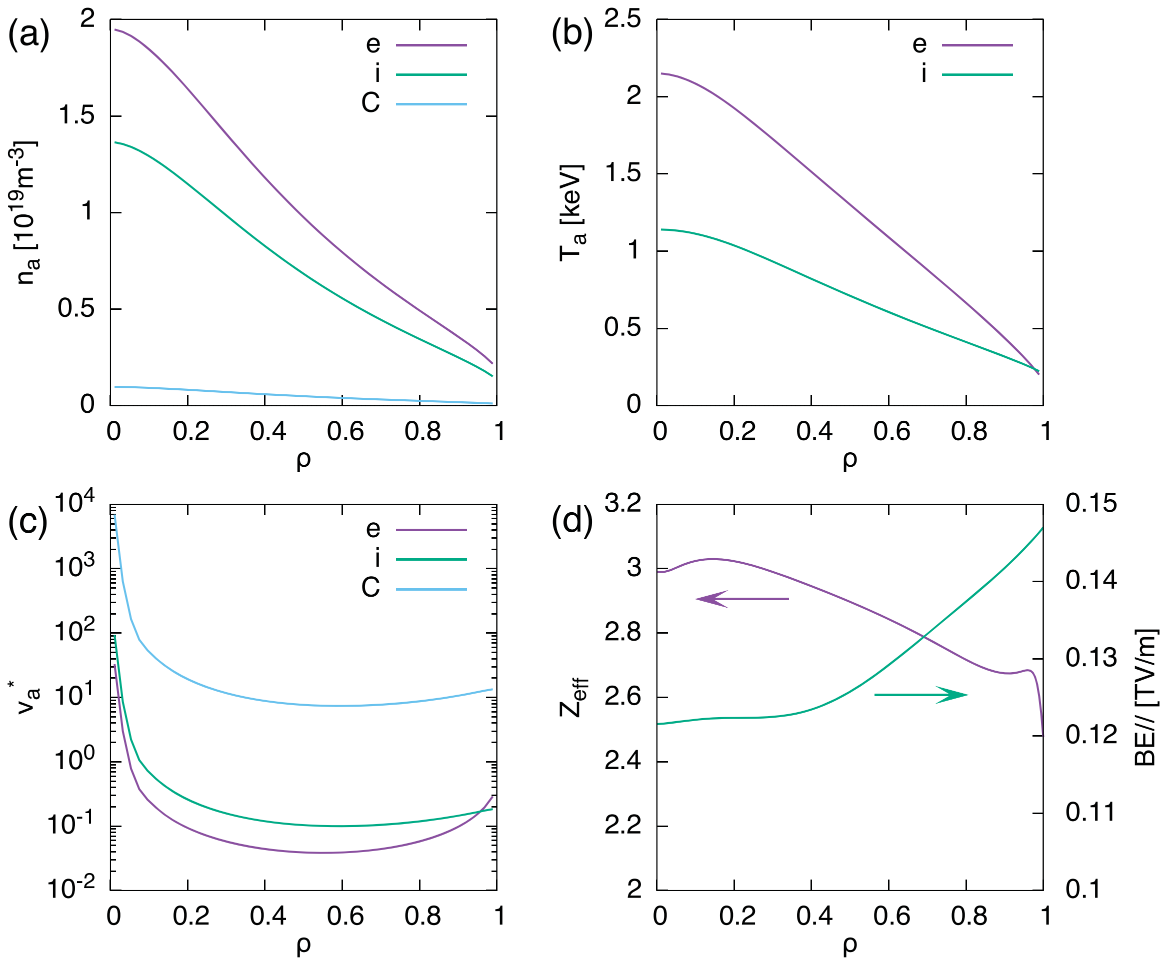

FIG. 1. The plasma profiles used in this study as a function of ρ, including (a) density, (b) temperature, (c) effective collisionality ν^*, and (d) the effective charge Z_eff, and the parallel electric field $\langle BE_\parallel \rangle$. The subscript a denotes an arbitrary species, and ρ is defined by the square root of the normalized toroidal flux.

The simulations were conducted using two different types of matrix elements regarding the collision operator. Case (A) utilized the elements derived from the Hirshman's model collision operator,[5] which satisfy both momentum conservation and the self-adjointness in general cases. Case (B) employed those derived from the exact linearized collision operator,[24,31,32] which satisfy momentum conservation but deviate to some extent the self-adjointness for different mass and temperature ratios between species. The theoretical and algebraic analysis has already shown that momentum conservation is the sole factor relevant to ambipolarity of the neoclassical particle fluxes, while the self-adjoint property has no impact on it. Therefore, it is expected that both cases should exhibit a similar degree of ambipolarity. Figure 2 illustrates the comparison of the neoclassical particle fluxes, multiplied with their respective charges, i.e., $e_a\Gamma_a^\psi$, between TASK/TX and MI for cases (A) and (B). In Figs. 2(a), the "sum" represents $\sum_a e_a\Gamma_a^\psi$, which is identical to those shown in Figs. 2(b): Figs. 2(b) provide a close-up view of the $\sum_a e_a\Gamma_a^\psi$ profiles shown in Figs. 2(a). It can be observed that the fluxes calculated by TASK/TX and MI exhibit good agreement for all species. The slight differences between them can be explained as follows. In reality, a TASK/TX simulation is unable to decompose the contributions to a particle flux. Consequently, all contributions are consistently combined to form the particle flux. Although turbulence is a prominent driver of particle flux, in this case, the simulation was allowed to proceed for only one time step after the forces responsible for turbulent transport were artificially deactivated. The resulting particle flux can be reasonably considered as primarily the neoclassical flux. However, considering the intricate nature of the governing equations in TASK/TX, other small influences inevitably come into play, causing a slight deviation of the resultant flux from a purely neoclassical flux.

In Figs. 2(a), it can be observed that ambipolarity, represented by the "sum," is satisfactorily maintained for both cases and both models. Even in the close-up views shown in Figs. 2(b), a minimal breakdown of ambipolarity is observed. TASK/TX is somewhat susceptible to numerical errors due to the need of computing large matrices, which could have relatively large off diagonal components, composed of simultaneous linearized equations with 41 unknowns. The influence of sources and scrape-off layers in the edge region could also contribute to non-negligible effects. Additionally, achieving ambipolarity requires charge neutrality, as seen in Eq. (27), but a TASK/TX simulation is never precisely charge neutral. $\sum_{a\neq e} e_a n_a - n_e$, evaluated as a measure of charge density balance, is shown in Figs. 2(c). The profile shape seems to be similar to $\sum_a e_a\Gamma_a^\psi$ calculated by MI, shown in Figs. 2(b). The slight breakdown of ambipolarity calculated by MI using the TASK/TX plasma profiles can thus be attributed to the issue of charge neutrality, which will be further examined in Sec. IV B. Ultimately, it can be stated that ambipolarity is well maintained in both TASK/TX and MI, regardless of whether it is case (A) or case (B). This numerical

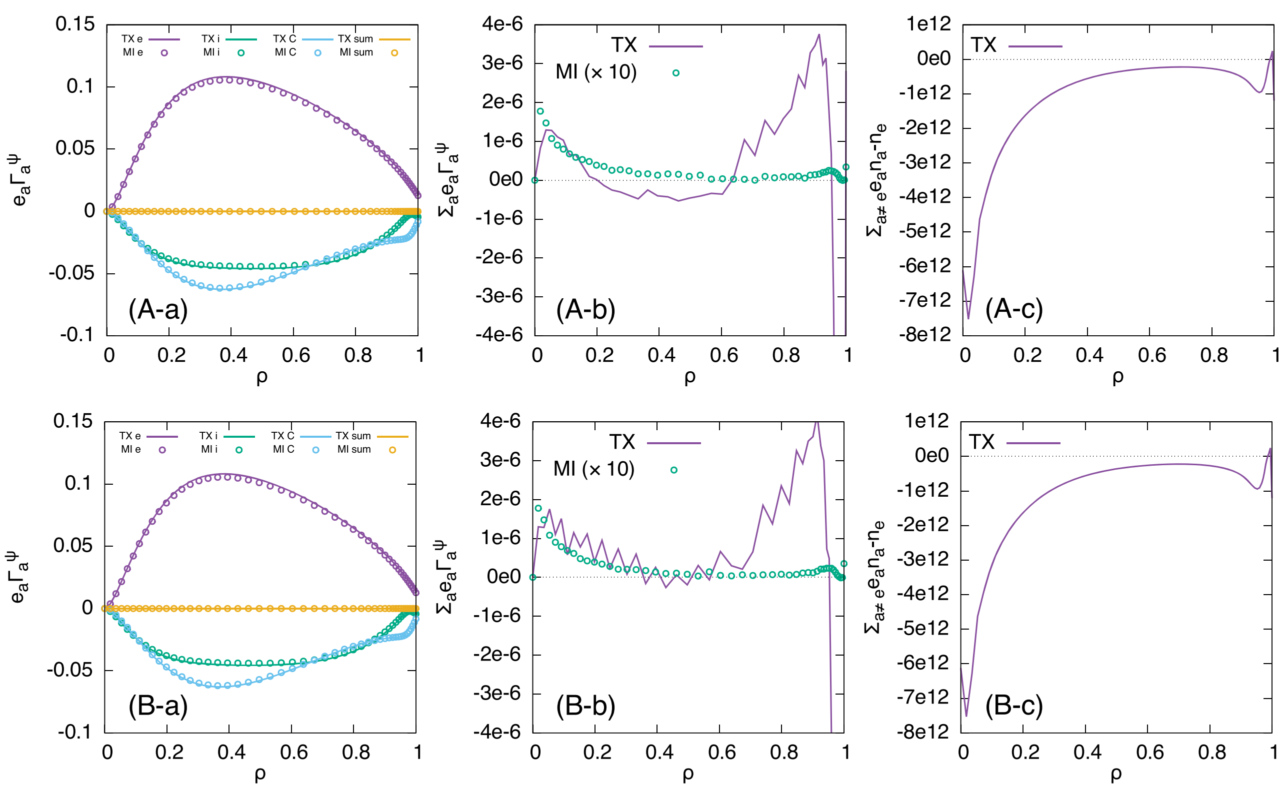

FIG. 2. Comparison of (a) the neoclassical particle fluxes and (b) ambipolarity between TASK/TX, drawn by solid lines, and MI, drawn by open circles. The figures (c) demonstrate the degree of charge density neutrality calculated in TASK/TX by evaluating $\sum_{a\neq e} e_a n_a - n_e$. (A-a) means (a) of case (A) using Hirshman's model operator, and the same labeling convention applies to (B), which uses the exact linearized operator. Note that the graphs in (b) are identical to those labeled as "sum" in (a), but with a different scale on the vertical axis. For better visibility, the MI results in figure (b) are multiplied by a factor of 10.

finding solidifies the fact that the self-adjointness does not play a role in ambipolarity. From another perspective, these numerical results affirm the reliability of the numerical implementation.

Another observation from Fig. 2 is that the magnitude of the electron particle flux is larger than that of the deuterium and carbon particle fluxes: $|\Gamma_{\rm e}^{\psi}| > |\Gamma_{\rm i}^{\psi}|, |Z_{\rm C}\Gamma_{\rm C}^{\psi}|$. This fact can only be explained by considering the contribution of the Ware flux based on theoretical considerations. In our setup, the finite $\langle BE_{\parallel}\rangle$ is present, which gives rise to the Ware flux. The $\langle BE_{\parallel}\rangle$ must have a significant impact, which will be elucidated in Sec. IV C.

B. Charge neutrality and ambipolarity

In Sec. IV A, it was mentioned that the tiny breakdown of ambipolarity in the particle fluxes calculated by MI is attributed to a small deviation from perfect charge neutrality. As previously discussed, achieving perfect charge neutrality is not possible in TASK/TX simulations due to the self-consistent nature, where a slight imbalance in charge densities leads to the generation of E_r according to Gauss's law. To address this issue, another code called CHARROT, which has already implemented MI, is utilized.[40,41] Based on neoclassical transport theory, CHARROT was originally developed to convert experimentally measured carbon toroidal rotation to deuterium toroidal rotation, which cannot usually be measured directly at least in JT-60U. It is capable of reading plasma profiles and equilibrium data and outputting various neoclassical transport quantities. In our case, TASK/TX provides the plasma profiles shown in Fig. 1 and the equilibrium data for CHARROT to read. Only the minimum required profile data for running CHARROT is outputted from TASK/TX, including $T_{\rm e}$, $T_{\rm i}$, $n_{\rm e}$, $Z_{\rm eff}$, $\langle BE_{\parallel}\rangle$, and carbon toroidal rotation $V_{\rm tC}$. Quantities related to charge neutrality, such as $n_{\rm e}$ and $Z_{\rm eff}$, as well as the charge numbers of deuterium and carbon, are important in this context. With exact charge neutrality imposed, CHARROT calculates the density profiles for deuterium and carbon, which slightly differ from those in TASK/TX. Using the matrix elements derived from the exact linearized collision operator, MI implemented in CHARROT computes the profiles of neoclassical particle fluxes shown in Fig. 3(a), which are virtually equivalent to those in Fig. 2(B-a). A slight difference in the shape of the particle flux profile near the last closed flux surface (LCFS) where $\rho = 1$ can be observed between Figs. 2(B-a) and 3(a). Upon closer inspection of Fig. 2(B-a), it can be seen that TASK/TX employs a higher concentration of radial grid points in the edge region to capture possible steep profile gradients more accurately. On the other hand, CHARROT just reads in, not calculates, kinetic profiles as input and does not require an accumulation of grid points even in the case that the profile shape may change significantly. Therefore, CHARROT adopts equally spaced grid points, and this difference in the way of choosing grid points is the cause of the difference in the profiles. Also, since only the minimum required quantities are read into CHARROT from TASK/TX, the fluxes may not match exactly, nor is it necessary for our purpose. Figure 3(b) demonstrates exact ambipolarity at the level of numerical rounding error. The relatively large roughness observed in $\sum_a e_a\Gamma_a^{\psi}$ near the magnetic axis could be attributed to the accuracy of the ψ-derivatives of the kinetic profiles utilized in the expressions of the thermodynamic forces. This finding indicates that the particle fluxes computed by MI strictly adhere to ambipolarity when employing matrix elements that satisfy momentum conservation, irrespective of the self-adjointness.

C. Influence of the parallel electric field on the particle flux

In order to gain a detailed understanding of the large electron neoclassical particle flux in Fig. 3(a), it is necessary to analyze the individual components of the flux. These components include the banana-plateau (bp), Pfirsch–Schlüter (ps), and Ware pinch (wp) fluxes, as explained in Sec. II. MI can individually calculate these components, but TASK/TX cannot. Figure 4 provides the breakdown of the particle flux for each species. From Figs. 4(a) and 4(b), it is evident that the contribution of electron flux is relatively small in the banana-plateau flux, which is driven by the viscous and friction forces, and negligibly small in the Pfirsch–Schlüter flux. This fact has already been theoretically explained, as mentioned earlier, and forms the basis for the impurity flux modeling in the previous work,[16] which balances impurity and main ion fluxes by disregarding the electron flux. On the other hand, when examining the Ware pinch flux that arises in the presence of $E_{\parallel}$, the electron flux is not clearly negligible, but rather exceeds the fluxes of main ions and impurities. It should be noted that the electron flux appears outward in Fig. 4(c) because it is actually $-e\Gamma_{\rm e}^{\psi}$. However, the flux itself $\Gamma_{\rm e}^{\psi}$ is directed inward, similar to $\Gamma_{\rm i}^{\psi}$ and $\Gamma_{\rm C}^{\psi}$. This is why this flux is referred to as the Ware "pinch." The magnitude of the Ware pinch flux surpasses that of the banana-plateau and

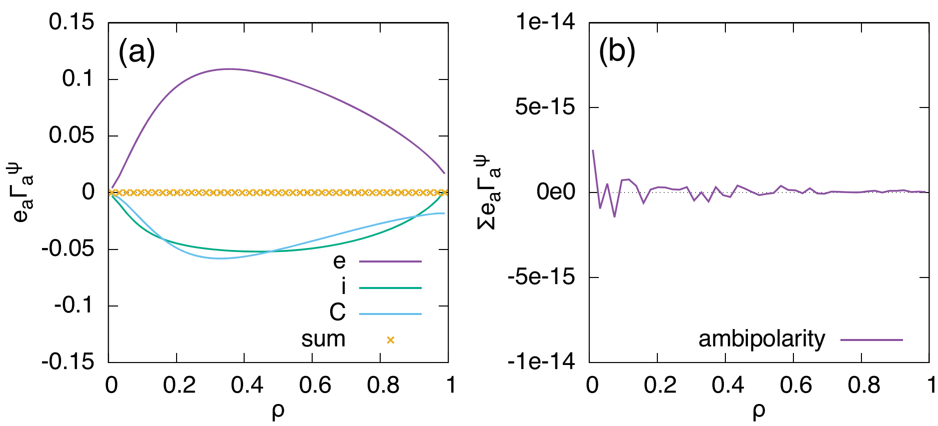

FIG. 3. (a) The neoclassical particle fluxes calculated in CHARROT using the profile output from TASK/TX. (b) The species sum of the particle fluxes multiplied by their respective charges for checking ambipolarity. Note that the graph in (b) is identical to the one labeled as "sum" in (a), but with a different scale on the vertical axis.

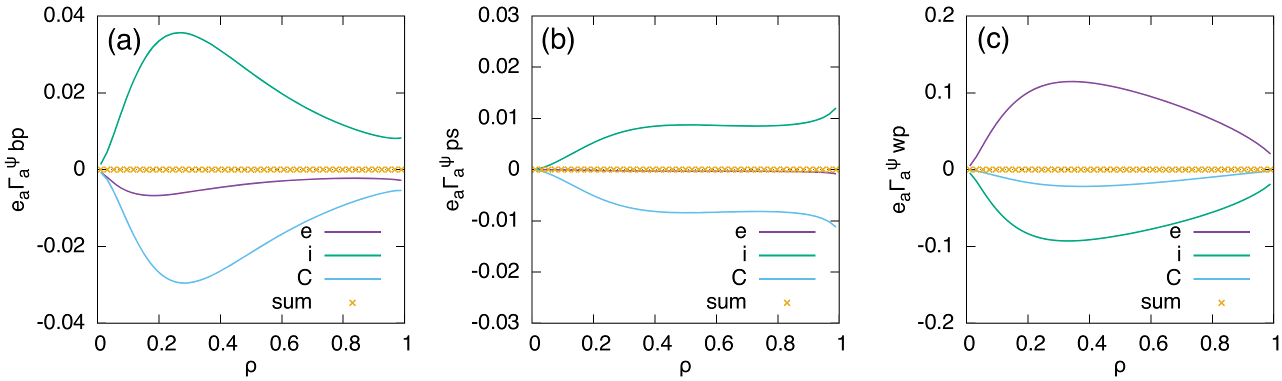

FIG. 4. Breakdown of the particle flux: (a) the banana-plateau (bp) flux, (b) the Pfirsch–Schlüter flux (ps), and (c) the Ware pinch (wp) flux.

Pfirsch–Schlüter fluxes, as one can see from the vertical axis scales of Fig. 4. Consequently, we understand the reason why the electron flux becomes prominent, even when compared to the main ion and impurity fluxes, as shown in Fig. 3(a). Finally, we also confirm that the detailed balanced principle is found to hold.

In our case, the spatial averaged value of $\langle BE_{\|}\rangle$ is roughly $0.13\,\mathrm{TV/m}$, as demonstrated in Fig. 1(d). This corresponds to a loop voltage of $V_{\mathrm{loop}} \sim 1\,\mathrm{V}$ at the LCFS. The significance of the Ware flux evidently relies on its magnitude. Thus, in order to observe the influence of the Ware flux in the total flux more clearly, we conducted a simulation by artificially reducing the input $\langle BE_{\|}\rangle$ by a factor of 10, i.e., $\langle BE_{\|}\rangle \sim 0.013\,\mathrm{TV/m}$ and $V_{\mathrm{loop}} \sim 0.1\,\mathrm{V}$. Even without performing a simulation, it can be predicted in advance from Eqs. (8) and (39) that by reducing $\langle BE_{\|}\rangle$ to one-tenth, the Ware flux will decrease by the same proportion without affecting other flux components. The simulation confirms that the outcomes presented in Fig. 5 align with

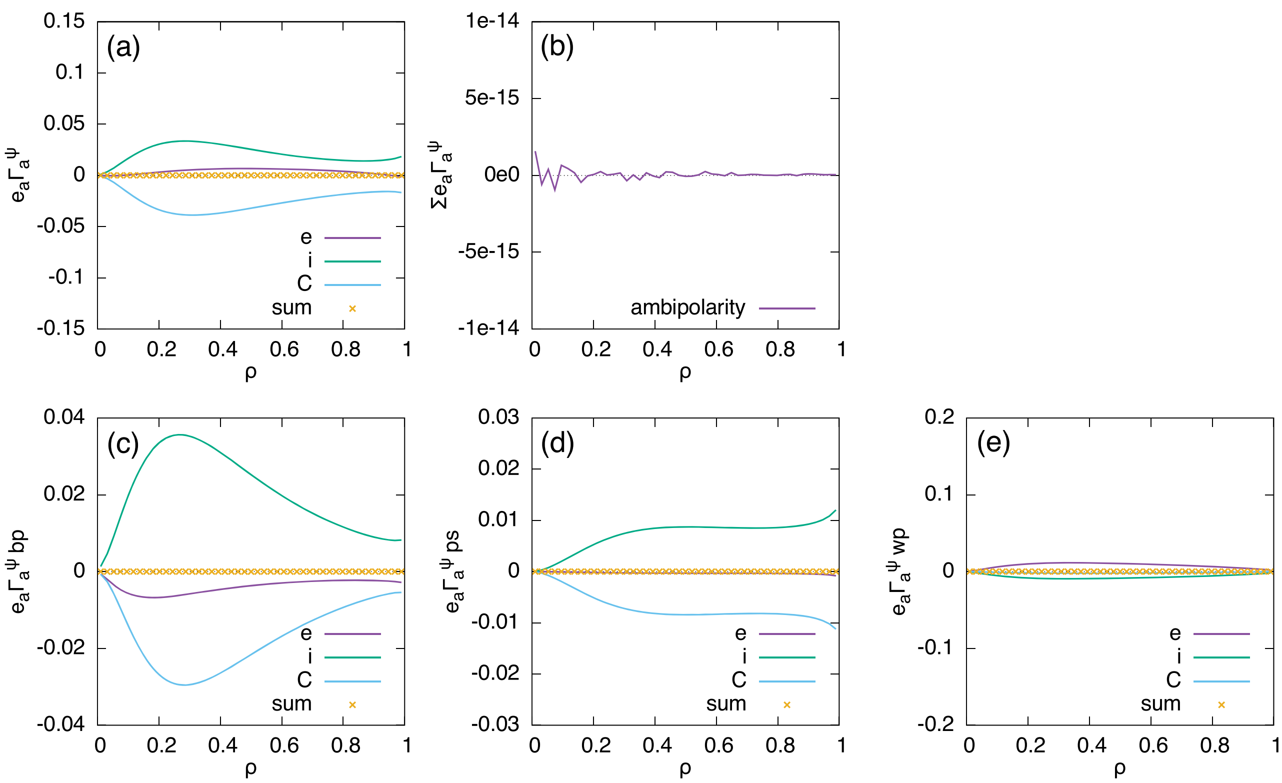

FIG. 5. In the case of $\langle BE_{\|}\rangle$, reduced by a factor of 10 compared to the original case corresponding to Figs. 3 and 4. (a) The neoclassical particle fluxes calculated in CHARROT using the profiles output from TASK/TX. (b) The species sum of the particle fluxes multiplied by their respective charges for checking ambipolarity. Profiles (c)–(e) show the breakdown of the particle flux exhibited in (a): (c) the banana-plateau (bp) flux, (d) the Pfirsch–Schlüter flux (ps), and (e) the Ware pinch (wp) flux.

this expectation. As a consequence of reducing the Ware flux to one-tenth, the electron flux is relatively minor compared to the main ion and impurity fluxes, as depicted in Fig. 5(a).

This result suggests that even with a loop voltage of standard tokamak operations, a substantial electron neoclassical particle flux, primarily consisting of the Ware flux, can be generated.

The L-mode plasma has been examined so far, but it is beneficial to confirm that the same conclusions apply to an H-mode plasma with a pedestal in the edge region. Similar to the procedure employed in the previous L-mode plasma case, a TASK/TX simulation was conducted to generate profiles for the H-mode plasma. The simulation procedure itself remained consistent, but some adjustments were made to form pedestals. These adjustments included increasing the plasma density, applying an equivalent amount of auxiliary heating to both electrons and ions, and intentionally decreasing turbulent heat diffusivities in the edge region to form temperature pedestals. Due to the assumption of the Prandtl number of unity, momentum diffusivities also exhibited a decrease in the peripheral region. The resultant plasma profiles used for assessment are presented in Fig. 6. As compared to the L-mode plasma shown in Fig. 1, the temperatures are higher, collisionalities are lower, and $\langle BE_\parallel \rangle$ is smaller. Also, the ion temperature is higher than the electron temperature, unlike the previous case.

As Figs. 7(a) and 7(b) demonstrate, the CHARROT calculation indicates that ambipolarity remains maintained even in the H-mode plasma. Due to the smaller parallel electric field and the larger temperature gradients, bulk ions exhibit outward transport, while electrons and impurities experience inward transport, similar to that seen in Fig. 5(a). Recall that since the electron charge e_e is negative, the positive $e_e\Gamma_e^\psi$ shown in Fig. 7(a) means that Γ_e^ψ is directed inward. The steep temperature and pressure gradients formed in the pedestal region lead to sharp peaks in the profiles of the banana-plateau and Pfirsch–Schlüter fluxes, which are driven by the thermodynamic forces A_1 and A_2, where $\rho \geq 0.9$, as seen in Figs. 7(c) and 7(d). On the other hand, the Ware flux, which is not driven by the gradients, does not show explicit influence from the pedestal structure, as confirmed in Fig. 7(e).

V. CONCLUSIONS AND PERSPECTIVES

Within the framework of the moment method, the roles of momentum conservation and the self-adjointness of the collision

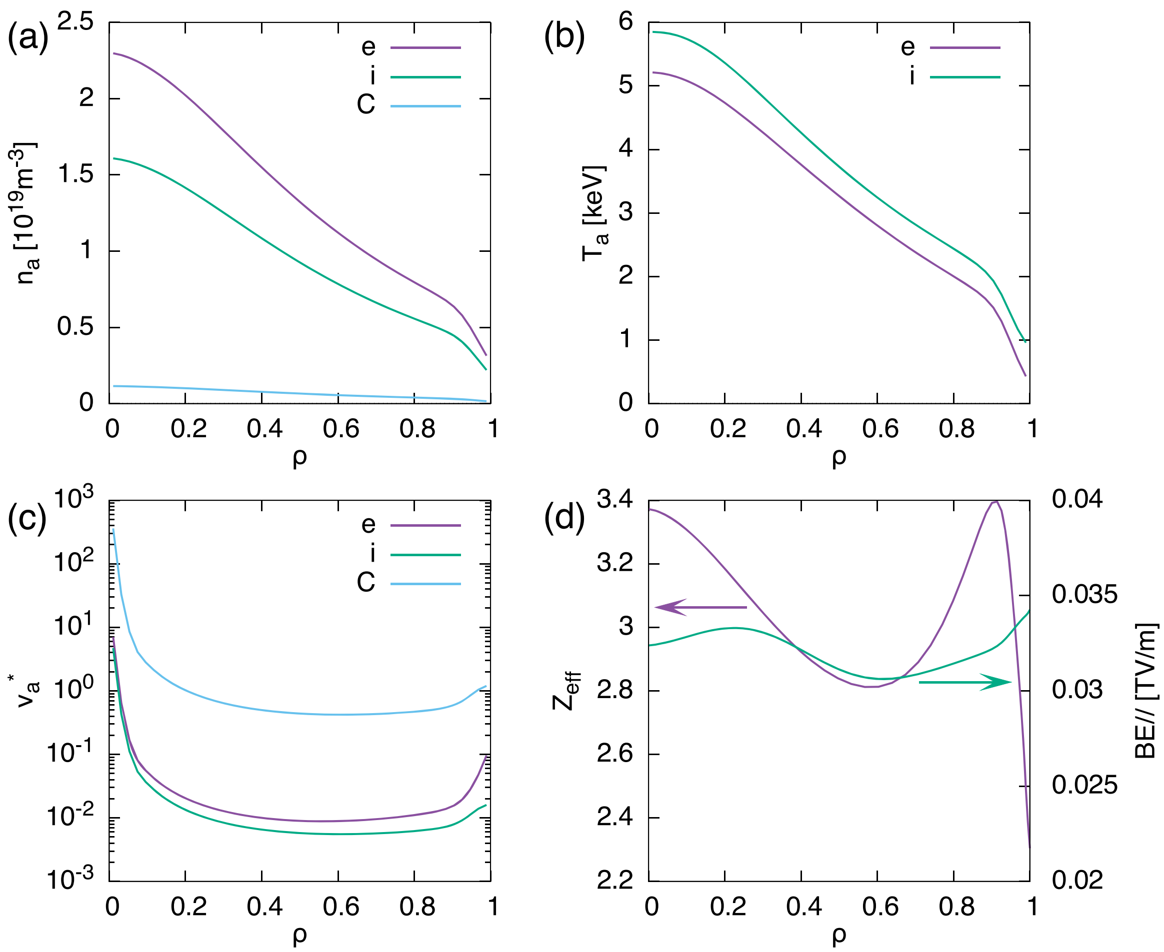

FIG. 6. The H-mode plasma profiles as a function of ρ, including (a) density, (b) temperature, (c) effective collisionality, and (d) the effective charge and the parallel electric field.

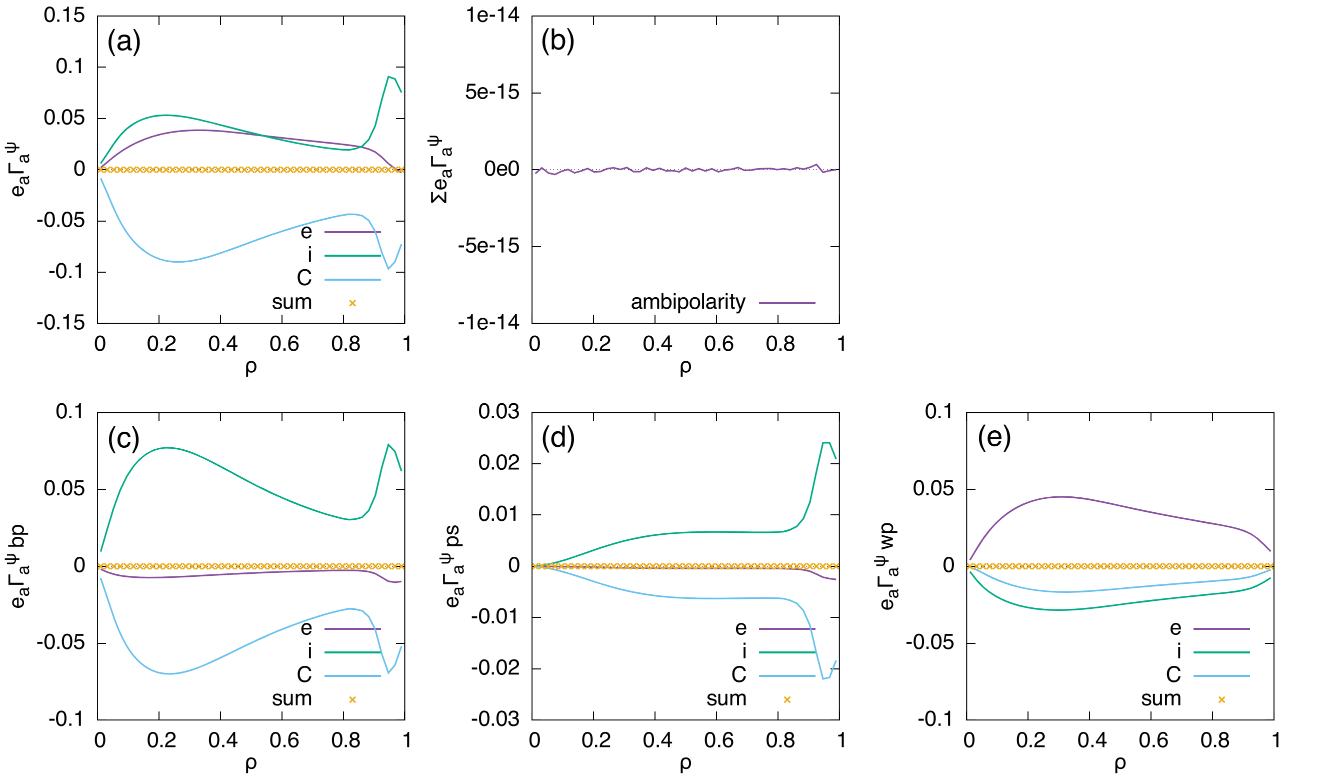

FIG. 7. In the case of the H-mode plasma compared to the L-mode plasma corresponding to Figs. 3 and 4. (a) The neoclassical particle fluxes calculated in CHARROT using the profiles output from TASK/TX. (b) The species sum of the particle fluxes multiplied by their respective charges for checking ambipolarity. Profiles (c)–(e) show the breakdown of the particle flux exhibited in (a): (c) the banana-plateau (bp) flux, (d) the Pfirsch–Schlüter flux (ps), and (e) the Ware pinch (wp) flux.

operator in the neoclassical particle flux were thoroughly investigated theoretically, algebraically, and numerically. As previously pointed out in the work,[5,38] it was theoretically demonstrated that in an axisymmetric system, momentum conservation is the sole contributor to maintaining ambipolarity, while the self-adjoint property does not play any role. By algebraically inverting the viscous and friction matrix, we have confirmed this fact. Just checking ambipolarity of the banana-plateau flux, as shown in Eq. (27), does not necessarily require calculating the inverse matrix. However, to clearly understand the important feature of the poloidal flow and particle flux being independent of E_r in an axisymmetric system, careful matrix calculations are needed. In other words, both momentum conservation and the self-adjointness are necessary to establish this fact. This finding is important because while the exact linearized collision operator guarantees momentum conservation, it does not guarantee the self-adjointness in a general case where colliding particles have different masses and temperatures. Momentum conservation alone ensures ambipolarity. Therefore, in the case using the exact linearized collision operator, explicitly excluding terms associated with E_r from the numerical implementation of the poloidal flow and particle flux in a transport code will avoid physical inconsistencies. This is indeed the approach followed in the actual numerical implementation.[6,7] Now, let us address the question of choosing between the two types of the improved Sugama operators.[22] From the standpoint of implementing the matrix elements in a transport code or a neoclassical transport solver, the emphasis should not be placed on the self-adjointness. Instead, it is preferable to use the model that reproduces the same friction–flow relations as those provided by the exact linearized collision operator.

In contrast, TASK/TX does not directly solve the algebraic equations that determine the poloidal flow and E_r. Instead, it self-consistently determines these quantities by solving a system of governing differential equations,[37] and the terms dependent on E_r cannot be excluded from the governing equations. Therefore, it is necessary to use matrix element expressions that preserve the self-adjointness in TASK/TX to ensure the consistency of the calculations.

In the presence of a finite $E_\parallel$, we have conducted a detailed investigation on the composition of each component of the neoclassical particle flux in the L-mode plasma. The banana-plateau flux and the Pfirsch–Schlüter flux exhibit nearly equal fluxes of outward main ions and inward impurities, respectively, with the electron flux being negligible. However, the inward Ware flux for each species can become substantial depending on the magnitude of $E_\parallel$. In a plasma with $V_{\mathrm{loop}} \sim 1\,\mathrm{V}$, the Ware flux is significantly larger than other components, whereas it is comparable to the Pfirsch–Schlüter flux when $V_{\mathrm{loop}} \sim 0.1\,\mathrm{V}$. In a typical tokamak plasma, where $E_\parallel$ exists, it is essential to consider the Ware flux, and therefore, the electron flux cannot be disregarded. This fact should be taken into account when modeling a neoclassical impurity flux. Finally, we have confirmed that the same conclusion reached in the L-mode plasma is applicable to the H-mode plasma as well.

Currently, neither TASK/TX nor MI have implemented the matrix element representation of the improved Sugama operator. The explicit description of this representation can be found in the paper,[22] and it will be incorporated into both codes in the near future.

ACKNOWLEDGMENTS

The author expresses his sincere gratitude to Professor H. Sugama for his helpful comments. This work was supported by JSPS KAKENHI, Grant No. 22K03574, and partly supported by the RIAM Joint Research 2023S2-CD-2.

AUTHOR DECLARATIONS

Conflict of Interest

The author has no conflicts to disclose.

Author Contributions

Mitsuru Honda: Conceptualization (lead); Data curation (lead); Formal analysis (lead); Funding acquisition (lead); Investigation (lead); Methodology (lead); Project administration (lead); Resources (lead); Software (lead); Supervision (lead); Validation (lead); Visualization (lead); Writing – original draft (lead); Writing – review & editing (lead).

DATA AVAILABILITY

The data that support the findings of this study are available from the corresponding author upon reasonable request.

APPENDIX: DERIVATION OF THE INDEPENDENCE OF $\hat{u}_{a\theta}$ FROM $\partial_\psi \Phi$ IN THE LIMIT OF SMALL VISCOSITIES

In the following, the parallel electric field is assumed to vanish, i.e., $\langle BE_\parallel \rangle = 0$. Since the smallness of Δ_a means that the viscous forces are much smaller than the friction forces, from Eqs. (25) and (26), we obtain

$$\langle BF_{a1\parallel} \rangle = \sum_b \left(\ell_{11}^{ab} \langle Bu_{b\parallel} \rangle - \frac{2}{5} \ell_{12}^{ab} \frac{\langle Bq_{b\parallel} \rangle}{p_b} \right) = 0, \tag{A1}$$

$$\langle BF_{a2\parallel} \rangle = \sum_b \left(-\ell_{21}^{ab} \langle Bu_{b\parallel} \rangle + \frac{2}{5} \ell_{22}^{ab} \frac{\langle Bq_{b\parallel} \rangle}{p_b} \right) = 0. \tag{A2}$$

The parallel friction force and the parallel heat friction force are nil for any species to zeroth order in Δ_a. Equation (14) obtained when both momentum conservation and the self-adjointness hold can be rewritten as

$$\ell_{i1}^{aa} = -\sum_{b \neq a} \ell_{i1}^{ab}, \tag{A3}$$

and it is then substituted into Eqs. (A1) and (A2) to obtain

$$-\sum_{b \neq a} \ell_{11}^{ab} (\langle Bu_{a\parallel} \rangle - \langle Bu_{b\parallel} \rangle) - \sum_b \left(\frac{2}{5} \ell_{12}^{ab} \frac{\langle Bq_{b\parallel} \rangle}{p_b} \right) = 0, \tag{A4}$$

$$\sum_{b \neq a} \ell_{21}^{ab} (\langle Bu_{a\parallel} \rangle - \langle Bu_{b\parallel} \rangle) + \sum_b \left(\frac{2}{5} \ell_{22}^{ab} \frac{\langle Bq_{b\parallel} \rangle}{p_b} \right) = 0. \tag{A5}$$

The solutions for which the above equations always hold are as follows:

$$\langle Bu_{a\parallel} \rangle = \langle Bu_{b\parallel} \rangle, \quad \text{for any } a \text{ and } b (\neq a), \tag{A6}$$

$$\langle Bq_{a\parallel} \rangle = 0, \quad \text{for any } a, \tag{A7}$$

and Eq. (A6) indicates that all the parallel particle flows must have the same value to this order. It is dubbed the common flow and is now written as

$$\langle Bu_{a\parallel} \rangle = \langle BV \rangle. \tag{A8}$$

Also, Eq. (A7) demonstrates that the common parallel heat flow does not exist.

As in Eq. (27), momentum conservation ensures that the species-sum of the parallel viscous force becomes nil. Hence, with Eqs. (15) and (21), we have

$$\begin{aligned} 0 &= \sum_a \langle \boldsymbol{B} \cdot \nabla \cdot \boldsymbol{\Pi}_a \rangle \\ &= \frac{3\langle (\boldsymbol{n} \cdot \nabla B)^2 \rangle}{\langle B^2 \rangle} \sum_a [\mu_{a1}(\langle BV \rangle - BV_{1a}) - \mu_{a2} BV_{2a}], \end{aligned} \tag{A9}$$

which leads to

$$\langle BV \rangle = \frac{\sum_a (\mu_{a1} BV_{1a} + \mu_{a2} BV_{2a})}{\sum_a \mu_{a1}}. \tag{A10}$$

This is the expression of the common flow. By substituting $\langle BV \rangle$ into $\langle Bu_{a\parallel} \rangle$ of Eq. (21), the poloidal flow can be expressed as

$$\begin{aligned} \hat{u}_{a\theta} &= \frac{1}{\langle B^2 \rangle} \left[\frac{\sum_b (\mu_{b1} BV_{1b} + \mu_{b2} BV_{2b})}{\sum_b \mu_{b1}} - BV_{1a} \right] \\ &= -\frac{I}{\langle B^2 \rangle} \left[\left(\sum_b \mu_{b1} \right)^{-1} \sum_b \left\{ \mu_{b1} \left(\frac{T_b}{e_b} \frac{\partial \ln p_b}{\partial \psi} + \frac{\partial \Phi}{\partial \psi} \right) \right. \right. \\ &\quad \left. \left. + \mu_{b2} \frac{T_b}{e_b} \frac{\partial \ln T_b}{\partial \psi} \right\} - \left(\frac{T_a}{e_a} \frac{\partial \ln p_a}{\partial \psi} + \frac{\partial \Phi}{\partial \psi} \right) \right] \\ &= -\frac{I}{\langle B^2 \rangle} \left[\left(\sum_b \mu_{b1} \right)^{-1} \sum_b \frac{T_b}{e_b} \left(\mu_{b1} A_1^b + \mu_{b2} A_2^b \right) - \frac{T_a}{e_a} A_1^a \right], \end{aligned} \tag{A11}$$

which apparently shows that the poloidal flow is independent of $\partial_\psi \Phi$.

REFERENCES

[1] M. Nakata and M. Honda, Plasmas Fusion Res. **17**, 1403083 (2022).
[2] C. Angioni, Plasma Phys. Control. Fusion **63**, 073001 (2021).
[3] A. A. Galeev and R. Z. Sagdeev, Sov. Phys. JETP **26**, 233 (1968), available at http://www.jetp.ras.ru/cgi-bin/e/index/e/26/1/p233?a=list.
[4] F. L. Hinton and R. D. Hazeltine, Rev. Mod. Phys. **48**, 239 (1976).

[5] S. P. Hirshman and D. J. Sigmar, Nucl. Fusion **21**, 1079 (1981).
[6] M. Kikuchi and M. Azumi, Plasma Phys. Controlled Fusion **37**, 1215–1238 (1995).
[7] W. A. Houlberg, K. C. Shaing, S. P. Hirshman, and M. C. Zarnstorff, Phys. Plasmas **4**, 3230 (1997).
[8] E. A. Belli and J. Candy, Plasma Phys. Controlled Fusion **50**, 095010 (2008).
[9] J. L. Velasco, I. Calvo, F. I. Parra, and J. M. García-Regaña, J. Comput. Phys. **418**, 109512 (2020).
[10] S. Satake, Y. Idomura, H. Sugama, and T.-H. Watanabe, Comput. Phys. Commun. **181**, 1069 (2010).
[11] S. Murakami, U. Gasparino, H. Idei, S. Kubo, H. Maassberg, N. Marushchenko, N. Nakajima, M. Romé, and M. Okamoto, Nucl. Fusion **40**, 693 (2000).
[12] W. X. Wang, W. M. Tang, F. L. Hinton, L. E. Zakharov, R. B. White, and J. Manickam, Comput. Phys. Commun. **164**, 178 (2004).
[13] S. Ku, C. S. Chang, M. Adams, J. Cummings, F. Hinton, D. Keyes, S. Klasky, W. Lee, Z. Lin, S. Parker, and CPES Team, J. Phys.: Conf. Ser. **46**, 87 (2006).
[14] E. D. Held, S. E. Kruger, J.-Y. Ji, E. A. Belli, and B. C. Lyons, Phys. Plasmas **22**, 032511 (2015).
[15] F. Hinton and S. K. Wong, Phys. Fluids **28**, 3082 (1985).
[16] C. Angioni and P. Helander, Plasma Phys. Controlled Fusion **56**, 124001 (2014).
[17] E. A. Belli, J. Candy, and C. Angioni, Plasma Phys. Controlled Fusion **56**, 124002 (2014).
[18] P. Maget, J. Frank, T. Nicolas, O. Agullo, X. Garbet, and H. Lütjens, Plasma Phys. Controlled Fusion **62**, 025001 (2020).
[19] K. C. Shaing, M. S. Chu, C. T. Hsu, S. A. Sabbagh, J. C. Seol, and Y. Sun, Plasma Phys. Controlled Fusion **54**, 124033 (2010).
[20] E. A. Belli and J. Candy, Plasma Phys. Controlled Fusion **57**, 054012 (2015).
[21] H. Sugama, T.-H. Watanabe, and M. Nunami, Phys. Plasmas **16**, 112503 (2009).
[22] H. Sugama, S. Matsuoka, S. Satake, M. Nunami, and T.-H. Watanabe, Phys. Plasmas **26**, 102108 (2019).
[23] M. Honda, M. Kikuchi, and M. Azumi, Nucl. Fusion **52**, 023021 (2012).
[24] M. Honda, Phys. Plasmas **21**, 092508 (2014).
[25] A. Ho, J. Citrin, C. D. Challis, C. Bourdelle, F. J. Casson, J. Garcia, J. Hobirk, A. Kappatou, D. L. Keeling, D. B. King, F. Koechl, E. Lerche, C. F. Maggi, J. Mailloux, and JET Contributors, Nucl. Fusion **63**, 066014 (2023).
[26] T. Luda, C. Angioni, M. G. Dunne, E. Fable, A. Kallenbach, N. Bonanomi, P. A. Schneider, M. Siccinio, G. Tardini, P. Rodriguez-Fernandez, J. W. Hughes, N. Howard, L. Frassinetti, S. Saarelma, T. A. U. Team, EUROfusion MST1 Team, Alcator C-Mod Team, and JET Contributors, Plasma Phys. Controlled Fusion **65**, 034001 (2023).
[27] I. Casiraghi, P. Mantica, R. Ambrosino, L. Aucone, B. Baiocchi, L. Balbinot, T. Barberis, A. Castaldo, M. Cavedon, L. Frassinetti, P. Innocente, F. Koechl, S. Nowak, P. Agostinetti, S. Ceccuzzi, L. Figini, G. Granucci, and P. Vincenzi, Plasma Phys. Controlled Fusion **65**, 035017 (2023).
[28] M. Honda, N. Aiba, H. Seto, E. Narita, and N. Hayashi, Nucl. Fusion **61**, 116029 (2021).
[29] E. Narita, M. Honda, M. Nakata, N. Hayashi, T. Nakayama, and M. Yoshida, Contrib. Plasma Phys. **63**, e202200152 (2023).
[30] S. P. Hirshman, Phys. Fluids **20**, 589 (1977).
[31] J.-Y. Ji and E. D. Held, Phys. Plasmas **13**, 102103 (2006).
[32] M. Taguchi, Phys. Plasmas **21**, 052504 (2014).
[33] E. A. Belli and J. Candy, Plasma Phys. Controlled Fusion **54**, 015015 (2012).
[34] M. Landreman, H. M. Smith, A. Mollén, and P. Helander, Phys. Plasmas **21**, 042503 (2014).
[35] J. A. Spencer, B. Adair, E. D. Held, J.-Y. Ji, and J. R. Jepson, J. Comput. Phys. **450**, 110862 (2022).
[36] M. Honda and A. Fukuyama, J. Comput. Phys. **227**, 2808 (2008).
[37] M. Honda and A. Fukuyama, Comput. Phys. Commun. **208**, 117 (2016).
[38] H. Sugama and W. Horton, Phys. Plasmas **3**, 304 (1996).
[39] S. P. Hirshman, Phys. Fluids **21**, 224 (1978).
[40] M. Honda, S. Ide, T. Takizuka, N. Hayashi, M. Yoshida, M. Yagi, and T. Fujita, Nucl. Fusion **54**, 073050 (2013).
[41] N. Aiba, M. Honda, and K. Kamiya, Nucl. Fusion **57**, 022011 (2017).